Covert Rate Study for Full-Duplex D2D Communications Underlaid Cellular Networks

Yihuai Yang, Bin Yang, Shikai Shen, Yumei She, and Tarik Taleb, *Senior Member, IEEE*

***Abstract*—Device-to-device (D2D) communications underlaid cellular networks have emerged as a promising network architecture to provide extended coverage and high data rate for various Internet of Things (IoT) applications. However, because of the inherent openness and broadcasting nature of wireless communications, such networks face severe risks of data privacy disclosure. This article investigates the covert communications in such networks for providing enhanced privacy protection. Specifically, this article explores the critical covert rate performance in a full-duplex (FD) D2D communication underlaid cellular network consisting of a base station, a cellular user, a D2D pair with a transmitter and an FD receiver, and a warden, where the D2D receiver (DR) can operate over either the FD mode or the half-duplex (HD) mode. We first derive transmission outage probabilities of cellular and D2D links under the FD and HD modes, respectively. Based on these probabilities, we further provide theoretical modeling for the covert rate under each mode and explore the corresponding covert rate maximization by jointly optimizing the transmit powers of the D2D pair and the cellular user. To improve the covert rate performance, we propose a general mode in which the DR can flexibly switch between these two modes. Under the general mode, we also investigate the theoretical modeling and maximization problems of covert rate. Finally, we present extensive numerical results to illustrate the covert rate performances under the FD, HD, and general modes.**

***Index Terms*—Covert rate, device-to-device (D2D) communications, full-duplex (FD), half-duplex (HD).**

Manuscript received 12 July 2022; revised 3 October 2022, 6 January 2023, and 27 February 2023; accepted 24 March 2023. Date of publication 6 April 2023; date of current version 24 August 2023. This work was supported in part by the National Natural Science Foundation of China under Grant 61962033 and Grant 62066023; in part by the Yunnan Province Science and Technology Joint Fund on Basic Research under Grant 202001BA070001-209; in part by the Academy of Finland Projects: 6Genesis under Grant 318927; in part by IDEA-MILL under Grant 335936; in part by the Natural Science Project of Anhui/Chuzhou University under Grant 2020qd16, Grant KJ2021ZD0128, and Grant 2022XJZD12; and in part by the Key Laboratory of Data Governance and Intelligent Decision in Universities of Yunnan. *(Corresponding authors: Shikai Shen; Bin Yang.)*

Yihuai Yang and Shikai Shen are with the School of Information Engineering, Kunming University, Kunming 650214, Yunnan, China (e-mail: Yihuai_Yang@126.com; kmssk2000@sina.com).

Bin Yang is with the School of Computer and Information Engineering, Chuzhou University, Chuzhou 239000, China, and also with the School of Information Engineering, Kunming University, Kunming 650214, Yunnan, China (e-mail: yangbinchi@gmail.com).

Yumei She is with the School of Mathematics and Computer Science, Yunnan Minzu University, Kunming 650500, Yunnan, China (e-mail: sheym1965@126.com).

Tarik Taleb is with the Information Technology and Electrical Engineering, University of Oulu, 90570 Oulu, Finland (e-mail: tarik.taleb@oulu.fi).

Digital Object Identifier 10.1109/JIOT.2023.3265275

I. Introduction

THE EXPLOSIVE growth of data traffic from massive Internet of Things (IoT) devices has placed an extremely heavy burden on cellular networks [1]. To address this challenge, device-to-device (D2D) communications underlaid cellular networks (DCNTs), which enable direct communications between nearby devices, have been identified as a promising technology to meet the rapidly growing data demand, in terms of increasing spectral efficiency, reducing latency, improving data rate, extending coverage, and enhancing power efficiency [2], [3], [4]. Such networks are opening new opportunities for IoT and also vehicle-to-vehicle (V2V) communications. However, due to the inherent features of wireless channels (e.g., broadcast and openness), the networks are facing serious security risks like eavesdropping attacks and privacy violations and thereby hindering their widespread deployment [5].

Covert communications, which intend to hide the existence of wireless communications, have emerged as exciting security technology to preserve users' privacy and also prevent wireless transmission content from being eavesdropped [6]. Such a security technology is highly appealing [7], especially, when the DCNTs are deployed to provide some critical services, such as military, healthcare, and location tracking. In these services, if an adversary cannot decide whether wireless communications occur or not, he does not know the transmitter's location achieving a higher level of privacy protection for the transmitter, and also has no opportunity to launch an eavesdropping attack. In DCNTs, the covert rate is a fundamental performance metric to measure the achievable data rate of covert communications. Therefore, it is of paramount importance to explore the covert rate in DCNTs.

By now, the covert rate is extensively studied in single-hop and two-hop/multiple-hop wireless networks (see Section II of Related Work). Notice that these results in the above works without the support of the base station (BS) cannot be applied to DCNTs because of the inherent characteristics (e.g., spectrum sharing and interference) of such networks. Some initial works have been devoted to the study of covert communications in DCNTs [8], [9], [10]. By sharing the same spectrum resource between cellular and D2D links, a transmit power control scheme for cellular and D2D transmitters was proposed in [8] with the goal of covert rate maximization of the D2D link. Using the dedicated orthogonal spectrum resource for D2D link, the work in [9] proposed a joint scheme of relay selection and transmit power control of D2D

transmitters to maximize the covert rate of cellular links. The work in [10] utilized jamming signals generated from an antenna array of BS to confuse the decision of the warden aiming to achieve covert communications of D2D link. An energy-efficient transmit probability-power control scheme for covert D2D communication was presented in the work [11], which takes into account the requirements with energy consumption and information freshness. Li et al. [12] investigated covert communications in the scenario of multiple wardens in D2D communications underlaid cellular networks. The work in [13] unitized the spectrum reusing technology to implement covert communications for D2D content sharing, based on the trust evaluation mechanism. Shi et al. [14] further investigated the content delivery mode selection and resource management for covert communications.

It is notable that the half-duplex (HD) and full-duplex (FD) are two fundamental communication modes. Under the HD mode, a receiver only receives messages from a transmitter at a specific time, while under the FD mode, the receiver can receive messages and send artificial noise for ensuring covertness simultaneously. In comparison with HD mode, such an FD mode can enhance covertness but may reduce the covert rate of D2D links due to the impact of self-interference. However, all aforementioned works in DCNTs consider the D2D receiver (DR) operates in HD mode. To fully address the advantages of the HD and FD modes, an important issue is how to conduct a joint study on these two modes. As a step toward this direction, this article designs a general mode to flexibly switch between the HD and FD modes for achieving covert rate improvement. Meanwhile, we also model the covert rate performance under the HD, FD, and general modes, respectively. Our study is of great importance to support security-sensitive applications in the sixth generation (6G) wireless networks, where a large number of wireless IoT devices can realize not only the short-range transmission of privacy data (e.g., patient's health information and financial data) but also the remote data transmission with the help of BS.

The contributions of this article are summarized as follows.

1) We first derive transmission outage probabilities of cellular and D2D links under the FD mode. Based on these probabilities, we model the covert rate of DCNT and further formulate the maximum covert rate as an optimization problem with the constraints of covertness requirement and the transmit powers of DT, DR, and cellular equipment (CE). We solve the optimization problem by optimizing these transmit powers.
2) We also derive the transmission outage probabilities of cellular and D2D links under the HD mode, model the covert rate and further, provide the formulation for the covert rate maximization problem with the constraints of covert requirement and the transmit powers of DT and CE. By optimizing these powers, we obtain the maximum covert rate with careful consideration of the self-interference issue.
3) We further propose a general model, where DR can flexibly switch between the FD and HD modes for improving the covert rate performance. Under such a general model, we also explore the theoretical covert rate and its maximization problem.
4) Extensive numerical results are presented to illustrate the covert rate and its maximum value by optimal power control under the FD, HD, and general modes.

TABLE I
ABBREVIATION AND NOTATIONS

Abbreviation /Notations	Description
D2D	Device-to-device
V2V	Vehicle-to-vehicle
IoT	Internet of Things
AWGN	Additive White Gaussian noise
FD	Full-duplex
HD	Half-duplex
DT	D2D transmitter
DR	D2D receiver
BS	Base station
WD	Warden
CE	Cellular equipment
C2B	Transmission from CE to BS
h_{ij}	Channel fading coefficient between nodes i and j
λ_{ij}	Exponential parameter for channel h_{ij}
ϕ	Self-interference cancellation coefficient
ε	Covertness requirement
$P_{\max}$	The maximum transmit power of DR
P_r, P_t, P_c	Transmit powers of DR, DT and CE, respectively
σ_w^2, σ_r^2, σ_b^2	Noise variances at WD, DR and BS, respectively
δ_r^{FD}, δ_b^{FD}	Transmission outage probabilities at DR and BS under FD mode, respectively
δ_r^{HD}, δ_b^{HD}	Transmission outage probabilities at DR and BS under HD mode, respectively
R_{FD}, R_{HD}	Desired rates under FD and HD modes, respectively

The remainder of this work is organized as follows. In Section II, we present the system model. Detection performance at the warden is studied in Section III. In Sections IV and V, we develop theoretical models on covert rate and related maximization problem under the FD and HD modes, respectively. The general mode is proposed in Section VI. Section V provides numerical results. Section VII concludes this article. The abbreviations and notations used in this article are given in Table I.

II. Related Work

For the single-hop wireless networks, a positive covert rate was proved to be achievable when the warden receives uncertain noise [15], [16], uncertain channel state information [17], [18], [19], and jamming signals [20], [21], [22]. Moreover, the work in [23] proposed joint design algorithms based on a penalty decomposition technique in a multiantenna Willie scenario to achieve the improvement of covert rates performance, while a multiantenna Alice Discrete-Time AWGN channel model was applied in [24] to achieve a positive covert rate without any uncertainty or jammer. Besides, the studies of covert communications have been extended to millimetre waves and Terahertz. The work in [25] adopted a beam training approach to establish a covert mmWave directional link and optimized the vital system parameters to maximize the covert rate. The work in [26] designed the covert beam training and covert data transmission in a multiuser mmWave communication system to maximize the covert rate. The work

of [27] explored the beamforming scheme based on a random frequency diverse array to enhance the performance of covert mmWave communications. In [28], a novel distance adaptive absorption peak modulation was proposed to enhance the covertness of the Terahertz (THz) covert communications. The work in [29] studied the optimality of Gaussian signaling for covert communications with the covertness constraint of the upper bound of Kullback–Leibler divergence. Regarding a finite number of channel uses, the work in [30] examined the delay-intolerant covert communications with fixed or random transmit power. Recently, regarding the space–air–ground integrated vehicular networks, the work in [17] applied improper Gaussian signaling techniques to reduce the co-channel interference and improve the covert rate performance of such networks. The work in [31] further explored the covert communications of unmanned aerial vehicles (UAVs) by joint optimization of their flying location and transmit power. Huang et al. [32], [33] and Li et al. [34] studied the covert video surveillance of ground-moving targets based on a UAV or a UAV team, while concealing the existence and movement of the UAVs from the targets' visual system. A 3-D location-based beamforming (LBB) scheme was proposed over the Rician channel to maximize the covert rate in [35]. The work in [36] initially focused on the timeless of warden's detection in the binary hypothesis test framework. The work of [37] investigated the optimum strategy of hiding the covert information onto the nonorthogonal multiple access (NOMA) information.

For the two-hop wireless networks, with the help of a relay, the positive covert rates were achievable [6], [38], [39], [40], [41]. Remarkably, intelligent reflecting surface (IRS), which is a promising solution to support energy-efficient and cost-effective covert communication, illustrates a huge potential to improve covert rate performance. Deng et al. [42] adopted two-way protocols in IRS-aided relaying networks to improve covert rate performance. An UAV-mounted IRS (UIRS) communication system over THz bands was also proposed to achieve the improvement of covert rate performance [43]. Chen et al. [44] and Wang et al. [45] utilized the integration of the IRS and the MIMO techniques to maximize the covert rate. The work [46] investigated the scenario that two-hop signals at the warden be combined to determine the presence of private transmission. Recently, a multihop relaying strategy was designed to improve covet rate performance [47], [48].

III. System Model

A. Network Model

As shown in Fig. 1, we consider a cellular network[1] consisting of a BS, a cellular user equipment (CE), a D2D pair with a transmitter (DT) and a receiver (DR), and a warden (WD). DT intends to covertly transmit confidential messages to DR, while WD tries to detect the existence of the covert transmission between DT and DR. DR can operate in HD mode or FD mode. Under the HD mode, DR can only receive messages. Under the FD mode, DR can receive and send messages simultaneously. Specially, DR can serve as a friendly jammer to confuse WD's detection via emitting artificial noise.

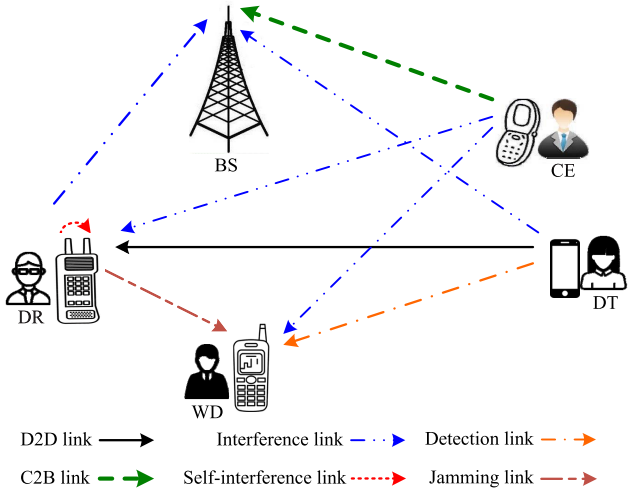

Fig. 1. System model.

We focus on the uplink transmission scenario in the concerned cellular network, where all transmissions use the uplink spectrum resource. Accordingly, there are six types of links in the network, namely, the link from DT to DR (D2D link), the link from CE to BS (C2B link), the interference link, the self-inference link from DR to itself, the detection link from DT to WD, and the jamming link from DR to WD. We consider that DR is equipped with two omnidirectional antennas for supporting the FD mode while each of the others has a single omnidirectional antenna. DR can adjust its transmit power P_r of artificial noise, which is no more than a maximum transmit power $P_{\max}$. CE and DT also employ adjustable transmission powers P_c and P_t, respectively. The maximum values of P_c and P_t are denoted as $P_{t\max}$ and $P_{c\max}$, respectively.

B. Channel Model

Similar to previous works [18], [49], [50], [51], this article considers that the time is slotted and all nodes are static from on time slot to another. A quasi-static Rayleigh fading channel is used to model these links as shown in Fig. 1, where the channel remains constant in a time slot and independently changes in different time slots. Let the subscripts t, r, c, b, and w denote the DT, DR, CE, BS, and WD, respectively. We use h_{tr}, h_{tb}, h_{tw}, h_{cr}, h_{cb}, h_{cw}, h_{rb}, h_{rw}, and h_{rr} to denote the fading coefficients of these links from DT to DR, DT to BS, DT to WD, CE to DR, CE to BS, CE to WD, DR to BS, DR to WD, and DR to DR, respectively.

We use h_{ij} to denote the channel fading coefficient between nodes i and j and use $(1/\lambda_{ij})$ to denote the mean of $|h_{ij}|^2$ over different time slots, where i and $j \in \{t, r, c, b, w\}$. The noise received at j is a complex additive Gaussian random variable with zero mean and variance σ_j^2, i.e., $n_j \sim \mathcal{CN}(0, \sigma_j^2)$.

[1]These works mainly consider simple scenarios where a transmitter attempts to covertly transmit the message to its receiver with/without a relay in the presence of a warden/multiple wardens [17], [18], [19], [20], [21], [22], [23], [24]. This is because it is very complex to determine the optimal detection error probability, the optimal detection threshold, and the optimal covert rate in the multiple-user scenario.

C. Full-Duplex Model

We consider DT and CE transmit signal over n available channel uses at each time slot. We use $y_r^{\mathrm{FD}}(i)$ and $y_b^{\mathrm{FD}}(i)$ to denote the received signal at DR and BS over the ith time slot. Under the FD mode, they can be given by

$$y_r^{\mathrm{FD}}(i) = \sqrt{P_t}h_{tr}x_t(i) + \sqrt{P_c}h_{cr}x_c(i) + \sqrt{\phi P_r}h_{rr}v_r(i) + n_r(i) \quad (1)$$

$$y_b^{\mathrm{FD}}(i) = \sqrt{P_t}h_{tb}x_t(i) + \sqrt{P_c}h_{cb}x_c(i) + \sqrt{P_r}h_{rb}v_r(i) + n_r(i) \quad (2)$$

where $x_t(i)$ and $x_c(i)$ denote the signal transmitted by DT and CE, respectively, $v_r(i)$ denotes the artificial noise generated by DR, and $E[|x_t(i)|^2] = E[|x_c(i)|^2] = E[|v_r(i)|^2] = 1$. Here, $E[\cdot]$ is the expectation operator and $i = 1, 2, \ldots, n$. ϕ $(0 < \phi \leq 1)$ denotes the self-interference cancellation coefficient corresponding to the cancellation level of the artificial noise signal. The transmit power of DR is treated as AN to cause uncertainty at the warden, which confuses the warden to determine whether the D2D transmitter transmits a message or not. To this end, the transmit power should be random for the warden. Thus, we regard it as a random variable following a continuous uniform distribution in this article. The assumption of the random variable on the AN has also been adopted in previous studies [49], [51], [52]. We use $f_{P_r}(x)$ to denote the probability density function (PDF) of the random variable, and then

$$f_{P_r}(x) = \begin{cases} \frac{1}{P_{\max}}, & \text{if } 0 \leq x \leq P_{\max} \\ 0, & \text{otherwise.} \end{cases} \quad (3)$$

Based on its received signal, WD performs a binary hypothesis test to decide whether or not DT did a covert transmission at a time slot. In this test, the null hypothesis (i.e., $\mathcal{H}_0$) states that DT did not transmit the covert message, while the alternative hypothesis (i.e., $\mathcal{H}_1$) states that DT did a covert transmission. Thus, the received signal at WD under these two hypotheses can be given by

$$\mathcal{H}_0 : y_w^{\mathrm{FD}}(i) = \sqrt{P_c}h_{cw}x_c(i) + \sqrt{P_r}h_{rw}v_r(i) + n_w(i) \quad (4)$$

and

$$\mathcal{H}_1 : y_w^{\mathrm{FD}}(i) = \sqrt{P_t}h_{tw}x_t(i) + \sqrt{P_c}h_{cw}x_c(i) + \sqrt{P_r}h_{rw}v_r(i) + n_w(i) \quad (5)$$

where $y_w^{\mathrm{FD}}(i)$ denotes the received signal at WD under the FD mode.

D. Half-Duplex Model

Under the HD mode, DR only receives messages without transmission at each time slot. We use $y_r^{\mathrm{HD}}(i)$ and $y_b^{\mathrm{HD}}(i)$ to denote the received signal at DR and BS under such a mode, respectively. Then, we have

$$y_r^{\mathrm{HD}}(i) = \sqrt{P_t}h_{tr}x_t(i) + \sqrt{P_c}h_{cr}x_c(i) + n_r(i) \quad (6)$$

and

$$y_b^{\mathrm{HD}}(i) = \sqrt{P_t}h_{tb}x_t(i) + \sqrt{P_c}h_{cb}x_c(i) + n_b(i). \quad (7)$$

Under the HD mode, WD also performs a binary hypothesis test to decide whether or not DR did a covert transmission. Then, we have

$$\mathcal{H}_0 : y_w^{\mathrm{HD}}(i) = \sqrt{P_c}h_{cw}x_c(i) + n_w(i) \quad (8)$$

and

$$\mathcal{H}_1 : y_w^{\mathrm{HD}}(i) = \sqrt{P_t}h_{tw}x_t(i) + \sqrt{P_c}h_{cw}x_c(i) + n_w(i) \quad (9)$$

where $y_w^{\mathrm{HD}}(i)$ denotes the received signal at WD under the HD mode.

E. Detection at Warden

Based on its received signals over the n channel uses, WD makes a binary decision on whether DT transmits covert messages or not under each of the FD and HD modes. The corresponding detection error probability ξ can be expressed as follows:

$$\xi = P(\mathcal{D}_1|\mathcal{H}_0) + P(\mathcal{D}_0|\mathcal{H}_1) \quad (10)$$

where $\mathcal{D}_1$ and $\mathcal{D}_0$ denote the binary decisions that WD conducts a covert transmission or not, respectively. $P(\mathcal{D}_1|\mathcal{H}_0)$ denotes the false alarm probability that $\mathcal{H}_0$ is true but WD makes a decision to approve $\mathcal{D}_1$. $P(\mathcal{D}_0|\mathcal{H}_1)$ denotes the miss detection probability that $\mathcal{H}_1$ is true but WD approves $\mathcal{D}_0$.

According to Pinsker's inequality [53], we have a lower bound of ξ given by

$$\xi \geq 1 - \sqrt{\frac{1}{2}\mathcal{D}(P_0\|P_1)} \quad (11)$$

where

$$\mathcal{D}(P_0\|P_1) = n\left[\ln(1+\gamma_w) - \frac{\gamma_w}{1+\gamma_w}\right]. \quad (12)$$

Here, $\mathcal{D}(P_0\|P_1)$ is the relative entropy between two probability distributions P_0 to P_1, and P_0 and P_1 are the probability distributions of WD's channel observations of n channel uses when $\mathcal{H}_0$ and $\mathcal{H}_1$ are true, respectively. γ_w is the signal-to-interference-plus-noise ratio (SINR) at WD. Note that when the value of $\mathcal{D}(P_0\|P_1)$ is small, the distance between these two distributions P_0 and P_1 is also small such that WD has a high detection error probability ξ.

In covert communications, we require a covert constraint $\xi \geq 1 - \varepsilon$, where ε is an arbitrarily small constant. We adopt $\mathcal{D}(P_0\|P_1)$ as covertness requirement, which is determined as follows:

$$\mathcal{D}(P_0\|P_1) \leq 2\varepsilon^2. \quad (13)$$

F. Performance Metrics

Covert rate is defined as the achievable rate from DT to DR, with which the transmission from DT to DR and that from CE to BS do not occur outage such that DR and BS can decode their received messages, while maintaining a high detection error probability at WD.

IV. Covert Rate Under Full-Duplex Mode

This section first provides theoretical modeling for the covert rate under FD mode, and then further explores the covert rate maximization.

A. Covert Rate Modeling

Based on the definition of covert rate, we have

$$\eta_{\mathrm{FD}} = R_{\mathrm{FD}}\left(1-\delta_r^{\mathrm{FD}}\right)\left(1-\delta_b^{\mathrm{FD}}\right) \tag{14}$$

where η_{FD} denotes the covert rate under FD mode, R_{FD} is a desired rate, δ_r^{FD} and δ_b^{FD} denote the transmission outage probabilities that DR and BS cannot successfully decode their received message, respectively. Specially, the transmission outage from CE to BS occurs when $C_{cb}^{\mathrm{FD}} < \zeta_{cb}$, and that from DT to DR occurs when $C_{tr}^{\mathrm{FD}} < \zeta_{tr}$. Here, ζ_{cb} and ζ_{tr} are two preset thresholds, C_{cb}^{FD} and C_{tr}^{FD} denote the channel capacity from CE to BS and that from DT to DR, respectively.

We need to determine the unknown δ_b^{FD} and δ_r^{FD}. To obtain them, we first give the SINRs at BS and DR, which are denoted by γ_b^{FD} and γ_r^{FD}, respectively. They are given by

$$\gamma_b^{\mathrm{FD}} = \frac{|h_{cb}|^2 P_c}{|h_{rb}|^2 P_r + |h_{tb}|^2 P_t + \sigma_b^2} \tag{15}$$

and

$$\gamma_r^{\mathrm{FD}} = \frac{|h_{tr}|^2 P_t}{\phi|h_{rr}|^2 P_r + |h_{cr}|^2 P_c + \sigma_r^2}. \tag{16}$$

Then, we obtain δ_r^{FD} and δ_b^{FD} in the following lemma.

Lemma 1: Under FD mode, the transmission outage probabilities δ_r^{FD} and δ_b^{FD} are determined as follows:

$$\delta_b^{\mathrm{FD}} = 1 - \frac{\lambda_{tb}\lambda_{rb}\exp\left(-\alpha\sigma_b^2\right)}{\alpha(P_t+\lambda_{tb})P_{\max}} \ln\frac{\alpha P_{\max}+\lambda_{tb}}{\lambda_{tb}} \tag{17}$$

and

$$\delta_r^{\mathrm{FD}} = 1 - \frac{\lambda_{rr}\lambda_{cr}\exp\left(-\beta\sigma_r^2\right)}{\beta^2\phi P_{\max}(P_c+\lambda_{cr})} \ln\frac{\beta\phi P_{\max}+\lambda_{rr}}{\lambda_{rr}} \tag{18}$$

where $\alpha = \lambda_{cb}(2^{\zeta_{cb}}-1)/P_c$, and $\beta = \lambda_{tr}(2^{\zeta_{tr}}-1)/P_t$.

Proof: We know that $|h_{ij}|^2$ is a random variable of exponential distribution with parameter λ_{ij}, and its PDF is given by

$$f_{|h_{ij}|^2}(x) = \lambda_{ij}e^{-\lambda_{ij}x} \tag{19}$$

where i and $j \in \{t, r, c, b, w\}$. Then, we can determine the transmission outage probability δ_b^{FD} as follows:

$$\begin{aligned}
\delta_b^{\mathrm{FD}} &= P\left(C_{cb}^{\mathrm{FD}} < \zeta_{cb}\right) \\
&= \mathrm{P}\left(\frac{|h_{cb}|^2 P_c}{|h_{rb}|^2 P_r + |h_{tb}|^2 P_t + \sigma_b^2} < 2^{\zeta_{cb}} - 1\right) \\
&= \int_0^{P_{\max}}\int_0^{\infty}\int_0^{\infty}\int_0^{\frac{\left(2^{\zeta_{cb}}-1\right)\left(|h_{rb}|^2P_r+|h_{tb}|^2P_t+\sigma_b^2\right)}{P_c}} \\
&\quad f_{|h_{cb}|^2}(x) f_{|h_{tb}|^2}(y) f_{|h_{rb}|^2}(z) f_{P_r}(w)\,dx\,dy\,dz\,dw \\
&= \int_0^{P_{\max}}\int_0^{\infty} \lambda_{tb}\left[1 - \frac{\lambda_{rb}\exp\left(-\alpha\left(zP_t+\sigma_b^2\right)\right)}{\alpha P_r + \lambda_{rb}}\right] \\
&\quad \exp(-\lambda_{tb}z) f_{P_r}(w)\,dz\,dw \\
&= \int_0^{P_{\max}}\left[1 - \frac{\lambda_{tb}\lambda_{rb}}{\alpha(\alpha P_r+\lambda_{rb})(P_t+\lambda_{tb})}\exp\left(-\alpha\sigma_b^2\right)\right] \\
&\quad f_{P_r}(w)\,dw \\
&= 1 - \frac{\lambda_{tb}\lambda_{rb}\exp\left(-\alpha\sigma_b^2\right)}{\alpha^2(P_t+\lambda_{tb})P_{\max}} \ln\frac{\alpha P_{\max}+\lambda_{rb}}{\lambda_{rb}}
\end{aligned} \tag{20}$$

where $\alpha = \lambda_{cb}(2^{\zeta_{cb}}-1)/P_c$.

We further determine the transmission outage probability δ_r^{FD} as follows:

$$\begin{aligned}
\delta_r^{\mathrm{FD}} &= P\left(C_{tr}^{\mathrm{FD}} < \zeta_{tr}\right) \\
&= \mathrm{P}\left(\frac{|h_{tr}|^2 P_t}{\phi|h_{rr}|^2 P_r + |h_{cr}|^2 P_c + \sigma_r^2} < 2^{\zeta_{tr}} - 1\right) \\
&= \int_0^{P_{\max}}\int_0^{\infty}\int_0^{\infty}\int_0^{\frac{\left(2^{\zeta_{tr}}-1\right)\left(\phi|h_{rr}|^2P_r+|h_{cr}|^2P_c+\sigma_r^2\right)}{P_t}} \\
&\quad f_{|h_{tr}|^2}(x) f_{|h_{rr}|^2}(y) f_{|h_{cr}|^2}(z) f_{P_r}(w)\,dx\,dy\,dz\,dw \\
&= \int_0^{P_{\max}}\int_0^{\infty}\left[1 - \frac{\lambda_{rr}\exp\left(-\beta\left(|h_{cr}|^2P_c+\sigma_r^2\right)\right)}{\beta\phi P_r + \lambda_{rr}}\right] \\
&\quad f_{|h_{cr}|^2}(z) f_{P_r}(w)\,dz\,dw \\
&= \int_0^{P_{\max}}\left[1 - \frac{\lambda_{rr}\lambda_{cr}}{\beta(\beta\phi P_r+\lambda_{rr})(P_c+\lambda_{cr})}\exp\left(-\beta\sigma_r^2\right)\right] \\
&\quad f_{P_r}(w)\,dw \\
&= 1 - \frac{\lambda_{rr}\lambda_{cr}\exp\left(-\beta\sigma_r^2\right)}{\beta^2\phi P_{\max}(P_c+\lambda_{cr})} \ln\frac{\beta\phi P_{\max}+\lambda_{rr}}{\lambda_{rr}}
\end{aligned} \tag{21}$$

where $\beta = \lambda_{tr}(2^{\zeta_{tr}}-1)/P_t$. We finish the proof of Lemma 1. ■

B. Covert Rate Maximization

Our goal is to maximize the covert rate under the FD mode by jointly optimizing the transmit powers of DT and CE and the AN power of DR. To this end, covert rate maximization can be formulated as the following optimization problem:

$$\max_{P_t,P_c,P_{\max}} \quad \eta_{\mathrm{FD}} \tag{22a}$$

$$\text{s.t.} \quad \mathcal{D}\left(P_0^{\mathrm{FD}} \| P_1^{\mathrm{FD}}\right) \le 2\varepsilon^2 \tag{22b}$$

$$0 \le P_t \le P_{t\max} \tag{22c}$$

$$0 \le P_c \le P_{c\max} \tag{22d}$$

$$0 \le P_{\max} \le P_{r\max} \tag{22e}$$

where (22b) represents the covert requirement, and (22c) and (22d) represent the ranges of transmit powers of DT and CE, respectively. Constraint (22e) represents that the range of the maximum transmit power of DR is between 0 and $P_{r\max}$.

Here

$$D\left(P_0^{\mathrm{FD}} \| P_1^{\mathrm{FD}}\right) = n\left[\ln\left(1+\gamma_w^{\mathrm{FD}}\right) - \frac{\gamma_w^{\mathrm{FD}}}{\gamma_w^{\mathrm{FD}}+1}\right] \tag{23}$$

where the SINR at WD under the FD mode is given by

$$\gamma_w^{\mathrm{FD}} = \frac{P_t|h_{tw}|^2}{P_c|h_{cw}|^2 + P_r|h_{rw}|^2 + \sigma_w^2} \tag{24}$$

and the terms $P_c|h_{cw}|^2$ and $P_r|h_{rw}|^2$ are the interference caused by CE and DR, respectively.

The solution to the optimization problem (22) is given in the following theorem.

Theorem 1: We use η_{FD}^* to denote the maximum covert rate, and use P_t^* and P_c^* to denote the optimal transmit powers of DT and CE, respectively. Then, we have

$$P_t^* = \frac{\varepsilon^2 + \sqrt{\varepsilon^4 + 2\varepsilon^2 n}}{n} \frac{|h_{cw}|^2 P_c^* + |h_{rw}|^2 P_r^* + \sigma_w^2}{|h_{tw}|^2} \tag{25}$$

$$P_c^* = \begin{cases} P_{c\max}, & \theta_1 \geq \theta_2 \\ 0, & \theta_1 < \theta_2 \end{cases} \tag{26}$$

where $\theta_1 = |h_{rr}|^2|h_{cw}|^2\phi P_r + \sigma_r^2|h_{cw}|^2$ and $\theta_2 = |h_{rw}|^2|h_{cr}|^2P_r + |h_{cr}|^2\sigma_w^2$.

Based on these optimal transmit powers, the maximum covert rate can be determined as follows:

$$\eta_{\mathrm{FD}}^* = R_{\mathrm{FD}}\frac{\lambda_{tb}\lambda_{rb}\lambda_{rr}\lambda_{cr}\exp\left[-\left(\alpha\sigma_b^2+\beta\sigma_r^2\right)\right]}{\alpha^2\beta^2\phi(P_t^*+\lambda_{tb})(P_c^*+\lambda_{cr})P_{\max}^2} \times \ln\left(\frac{\alpha P_{\max}+\lambda_{rb}}{\lambda_{rb}}\right)\ln\left(\frac{\beta\phi P_{\max}+\lambda_{rr}}{\lambda_{rr}}\right) \tag{27}$$

where $\alpha = \lambda_{cb}(2^{\zeta_{cb}}-1)/P_c^*$ and $\beta = \lambda_{tr}(2^{\zeta_{tr}}-1)/P_t^*$.

V. Covert Rate Under Half-Duplex Mode

In this section, we first provide the theoretical modeling for covert rate and then explore the covert rate maximization by optimizing the transmit powers of DT and CE under the HD mode.

A. Covert Rate Modeling

Under the HD mode, the covert rate η_{HD} can be expressed as follows:

$$\eta_{\mathrm{HD}} = R_{\mathrm{HD}}\left(1-\delta_r^{\mathrm{HD}}\right)\left(1-\delta_b^{\mathrm{HD}}\right) \tag{28}$$

where R_{HD} is a desired rate, δ_r^{HD} and δ_b^{HD} denote the transmission outage probabilities at DR and BS cannot successfully decode their received message, respectively. If $C_{cb}^{\mathrm{HD}} < \zeta_{cb}$, the transmission outage from CE to BS occurs. If $C_{tr}^{\mathrm{HD}} < \zeta_{tr}$, the transmission outage from DT to DR occurs. C_{cb}^{HD} and C_{tr}^{HD} denote the channel capacity from CE to BS and that from DT to DR, respectively.

We need to determine the unknown δ_b^{HD} and δ_r^{HD}. First, we use γ_b^{HD} and γ_r^{HD} to denote the SINRs at BS and DR, respectively. The SINRs are given by

$$\gamma_b^{\mathrm{HD}} = \frac{|h_{cb}|^2P_c}{|h_{tb}|^2P_t+\sigma_b^2} \tag{29}$$

and

$$\gamma_r^{\mathrm{HD}} = \frac{|h_{tr}|^2P_t}{|h_{cr}|^2P_c+\sigma_r^2}. \tag{30}$$

We can obtain the transmission outage probabilities δ_b^{HD} and δ_r^{HD} in the following lemma.

Lemma 2: Under the HD mode, the transmission outage probabilities at BS and DR can be determined as follows:

$$\delta_b^{\mathrm{HD}} = 1-\frac{\lambda_{tb}\exp\left(-\alpha\sigma_b^2\right)}{\alpha P_t+\lambda_{tb}} \tag{31}$$

and

$$\delta_r^{\mathrm{HD}} = 1-\frac{\lambda_{cr}\exp\left(-\beta\sigma_r^2\right)}{\beta P_c+\lambda_{cr}} \tag{32}$$

where $\alpha = \lambda_{cb}(2^{\zeta_{cb}}-1)/P_c$ and $\beta = \lambda_{tr}(2^{\zeta_{tr}}-1)/P_t$.

Proof: We first determine δ_b^{HD} as follows:

$$\begin{aligned}\delta_b^{\mathrm{HD}} &= P\left(C_{cb}^{\mathrm{HD}} < \zeta_{cb}\right) \\ &= \mathrm{P}\left(\frac{|h_{cb}|^2P_c}{|h_{tb}|^2P_t+\sigma_b^2} < 2^{\zeta_{cb}}-1\right) \\ &= \int_0^{\infty}\int_0^{\frac{\left(2^{\zeta_{cb}}-1\right)\left(|h_{tb}|^2P_t+\sigma_b^2\right)}{P_c}} f_{|h_{cb}|^2}(x)f_{|h_{tb}|^2}(y)dxdy \\ &= \int_0^{\infty}\left[1-\exp\left(-\alpha\left(|h_{tb}|^2P_t+\sigma_b^2\right)\right)\right]f_{|h_{tb}|^2}(y)dy \\ &= \int_0^{\infty}\lambda_{tb}\left[1-\exp\left(-\alpha\left(P_ty+\sigma_b^2\right)\right)\right]\exp(-\lambda_{tb}y)dy \\ &= 1-\frac{\lambda_{tb}\exp\left(-\alpha\sigma_b^2\right)}{\alpha P_t+\lambda_{tb}}\end{aligned} \tag{33}$$

where $\alpha = \lambda_{cb}(2^{\zeta_{cb}}-1)/P_c$.

We then determine δ_r^{HD} as

$$\begin{aligned}\delta_r^{\mathrm{HD}} &= P(C_{tr} < \zeta_{tr}) \\ &= \mathrm{P}\left(\frac{|h_{tr}|^2P_t}{|h_{cr}|^2P_c+\sigma_r^2} < 2^{\zeta_{tr}}-1\right) \\ &= \int_0^{\infty}\int_0^{\frac{\left(2^{\zeta_{tr}}-1\right)\left(|h_{cr}|^2P_c+\sigma_r^2\right)}{P_t}} f_{|h_{tr}|^2}(x)f_{|h_{cr}|^2}(y)dxdy \\ &= \int_0^{\infty}\left[1-\exp\left(-\beta\left(P_cy+\sigma_r^2\right)\right)\right]\lambda_{cr}\exp(-\lambda_{cr}y)dy \\ &= 1-\lambda_{cr}\exp\left(-\beta\sigma_r^2\right)\int_0^{\infty}\exp(-(\beta P_c+\lambda_{cr})y)dy \\ &= 1-\frac{\lambda_{cr}\exp\left(-\beta\sigma_r^2\right)}{\beta P_c+\lambda_{cr}}\end{aligned} \tag{34}$$

where $\beta = \lambda_{tr}(2^{\zeta_{tr}}-1)/P_t$.

We finish the proof of Lemma 2. ∎

B. Covert Rate Maximization

We aim to maximize the covert rate under the HD mode by jointly optimizing the transmit powers of DT and CE and thus, formulate the covert rate maximization as the following optimization problem:

$$\max_{P_t,P_c} \quad \eta_{\mathrm{HD}} \tag{35a}$$

$$\text{s.t.} \quad \mathcal{D}\left(P_0^{\mathrm{HD}}\|P_1^{\mathrm{HD}}\right) \leq 2\varepsilon^2 \tag{35b}$$

$$0 \leq P_t \leq P_{t\max} \tag{35c}$$

$$0 \leq P_c \leq P_{c\max} \tag{35d}$$

where (35b) represents the covert requirement, and (35c) and (35d) represent the ranges of transmit powers of DT and CE, respectively. In (35b), we have

$$D\left(P_0^{\mathrm{HD}}\|P_1^{\mathrm{HD}}\right) = n\left[\ln\left(1+\gamma_w^{\mathrm{HD}}\right)-\frac{\gamma_w^{\mathrm{HD}}}{\gamma_w^{\mathrm{HD}}+1}\right] \tag{36}$$

where

$$\gamma_w^{\mathrm{HD}} = \frac{P_t|h_{tw}|^2}{P_c|h_{cw}|^2+\sigma_w^2} \tag{37}$$

is the SINR at WD under HD mode.

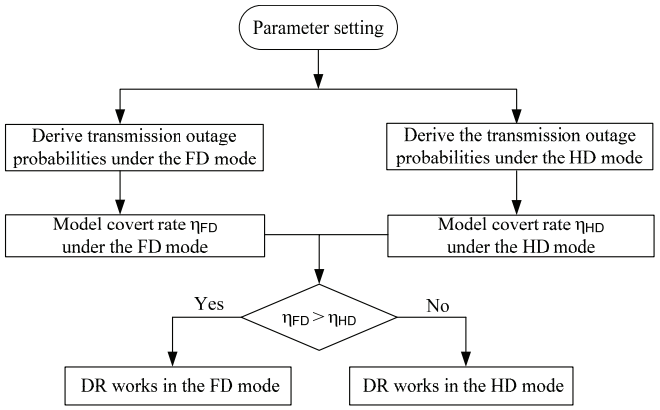

Fig. 2. System structure diagram of the general mode.

We can obtain the solution of the optimization problem (35) in the following theorem.

Theorem 2: Under the HD mode, the optimal transmit powers of DT and CE can be determined as follows:

$$P_t^* = \frac{\varepsilon^2 + \sqrt{\varepsilon^4 + 2\varepsilon^2 n}}{n} \cdot \frac{|h_{cw}|^2 P_c^* + \sigma_w^2}{|h_{tw}|^2} \tag{38}$$

and

$$P_c^* = \begin{cases} P_{c\max}, & \theta_3 \geq \theta_4 \\ 0, & \theta_3 < \theta_4 \end{cases} \tag{39}$$

where $\theta_3 = |h_{cw}|^2\sigma_r^2$ and $\theta_4 = |h_{cr}|^2\sigma_w^2$.

Based on these optimal transmit powers, we further determine the maximum covert rate η_{HD}^* as

$$\eta_{\mathrm{HD}}^* = R_{\mathrm{HD}} \frac{\lambda_{cr}\lambda_{tb}\exp\left[-\left(\alpha\sigma_b^2 + \beta\sigma_r^2\right)\right]}{(\alpha P_t^* + \lambda_{tb})(\beta P_c^* + \lambda_{cr})} \tag{40}$$

where $\alpha = \lambda_{cb}(2^{\zeta_{cb}} - 1)/P_c^*$ and $\beta = \lambda_{tr}(2^{\zeta_{tr}} - 1)/P_t^*$.

VI. Covert Rate Under General Mode

In this section, we propose a general mode. Under the general mode, the DR can flexibly switch between the FD and HD modes. Such a general mode can well overcome the passive impact of strong self-interference on covert performance under the FD mode. The system structure diagram of the general mode is shown in Fig. 2. and the covert rate optimization algorithm under the general mode is described in Algorithm 1. Regarding the time complexity of the algorithm, we have obtained the closed-form solutions for the maximum covert rate under the FD and HD modes (see Theorems 1 and 2). Thus, the complexity of the algorithm is a constant $O(1)$.

A. Covert Rate Modeling

The covert rate under the general mode can be expressed as follows:

$$\eta = \max\{\eta_{\mathrm{FD}}, \eta_{\mathrm{HD}}\}. \tag{41}$$

Algorithm 1 Covert Rate Optimization Algorithm Under the General Mode

Input:

P_r, P_t, P_c: Transmit powers of DR, DT and CE, respectively.

$h_{xy}, x, y \in \{t, r, b, w, c\}$: The channel fading coefficients.

$\sigma_w^2, \sigma_b^2, \sigma_r^2$: The noise variances at WD, DR and BS, respectively.

Output:

η^*: The optimal covert rate under the general mode.

/ Calculate the maximum covert rate η_{FD}^* under the FD mode */*

Calculate the SINRs at BS and DR, i.e. γ_b^{FD} and γ_r^{FD} under FD mode, respectively;

According to γ_b^{FD} and γ_r^{FD}, calculate the transmission outage probabilities δ_b^{FD} and δ_r^{FD}, respectively;

Calculate the covert rate $\eta_{\mathrm{FD}} = R_{\mathrm{FD}}(1-\delta_r^{\mathrm{FD}})(1-\delta_b^{\mathrm{FD}})$ under the FD mode;

Calculate η_{FD}^* according to (46);

/ Calculate the maximum covert rate η_{HD}^* under the HD mode */*

Calculate the SINRs at BS and DR, i.e. γ_b^{HD} and γ_r^{HD} under HD mode, respectively;

According to γ_b^{HD} and γ_r^{HD}, calculate the transmission outage probabilities δ_b^{HD} and δ_r^{HD}, respectively;

Calculate the covert rate $\eta_{\mathrm{HD}} = R_{\mathrm{HD}}(1-\delta_r^{\mathrm{HD}})(1-\delta_b^{\mathrm{HD}})$ under the HD mode;

Calculate η_{HD}^* according to (46);

/ Calculate the maximum covert rate η^* under the general mode */*

if $\eta_{\mathrm{FD}}^* \geq \eta_{\mathrm{HD}}^*$ **then**

  $\eta^* = \eta_{\mathrm{FD}}^*$

else

  $\eta^* = \eta_{\mathrm{HD}}^*$

end if

Here, by substituting (17) and (18) into (14), η_{FD} can be determined as follows:

$$\eta_{\mathrm{FD}} = R_{\mathrm{FD}} \frac{\lambda_{tb}\lambda_{rb}\lambda_{rr}\lambda_{cr}\exp\left[-\left(\alpha\sigma_b^2 + \beta\sigma_r^2\right)\right]}{\alpha^2\beta^2\phi(P_t + \lambda_{tb})(P_c + \lambda_{cr})P_{\max}^2} \times \ln\left(\frac{\alpha P_{\max} + \lambda_{rb}}{\lambda_{rb}}\right)\ln\left(\frac{\beta\phi P_{\max} + \lambda_{rr}}{\lambda_{rr}}\right) \tag{42}$$

and by substituting (31) and (32) into (28), η_{HD} can be determined as

$$\eta_{\mathrm{HD}} = R_{\mathrm{HD}} \frac{\lambda_{tb}\lambda_{cr}\exp\left[-\left(\alpha\sigma_b^2 + \beta\sigma_r^2\right)\right]}{(\alpha P_t + \lambda_{tb})(\beta P_c + \lambda_{cr})} \tag{43}$$

where $\alpha = \lambda_{cb}(2^{\zeta_{cb}} - 1)/P_c$ and $\beta = \lambda_{tr}(2^{\zeta_{tr}} - 1)/P_t$.

B. Covert Rate Maximization

The objective is to maximize the covert rate under the general mode, while being subject to the covertness requirement and transmit power constraints. The covert rate maximization can be formulated as the following optimization problem:

$$\max_{P_t, P_c, P_{\max}} \quad \eta \tag{44a}$$

TABLE II
PARAMETERS

Parameters	Values
Exponential parameter for channel h_{ij}, (λ_{ij})	1
Self-interference cancellation coefficient (ϕ)	0.05
Covertness requirement (ε)	0.01
The maximum transmit power of DR ($P_{\max}$)	2.0 W
Transmit powers of DR, DT and CE (P_r, P_t, P_c)	1.0 W
Variance noises at WD, DR and BS (σ_w^2, σ_r^2, σ_b^2)	0.001 W
Rates under FD and HD modes (R_{FD}, R_{HD})	1.5 Mbits/Channel

$$\text{s.t.} \quad \mathcal{D}(P_0\|P_1) \le 2\varepsilon^2 \tag{44b}$$
$$0 \le P_t \le P_{t\max} \tag{44c}$$
$$0 \le P_c \le P_{c\max} \tag{44d}$$
$$0 \le P_{\max} \le P_{r\max} \tag{44e}$$

where (44b) represents the covert requirement, and (44c) and (44d) represent the ranges of transmit powers of DT and CE, respectively. While, (44e) represents the range of the maximum AN power.

For the optimization problem in (45), the maximum covert rate can be expressed as follows:

$$\eta^* = \max\left\{\eta_{\text{FD}}^*, \eta_{\text{HD}}^*\right\} \tag{45}$$

where η_{FD}^* and η_{HD}^* are given in Theorems 1 and 2, respectively.

Regarding the tradeoff among the data rate, energy efficiency, and covert rate, we formulate covert rate maximization as the following optimization problem with the constraints of the data rate of cellular link and total power of transmitters under the general model

$$\max_{P_t,P_c,P_{\max}} \quad \eta \tag{46a}$$
$$\text{s.t.} \quad \mathcal{D}(P_0\|P_1) \le 2\varepsilon^2 \tag{46b}$$
$$0 \le P_t \le P_{t\max} \tag{46c}$$
$$0 \le P_c \le P_{c\max} \tag{46d}$$
$$0 \le P_{\max} \le P_{r\max} \tag{46e}$$
$$0 \le R_c \le R_{c\max} \tag{46f}$$
$$0 \le P_t + P_c \le P_{\text{all}} \tag{46g}$$

where (46f) represents the range of data rate of cellular link, and (46g) represents the range of the total power of transmitters DT, and CE. Here, $R_{c\max}$ represents the maximum value of the date rate, and P_{all} represents the maximum value of the total power of P_t and P_c. A 3-D search over $(P_c, P_t, P_{\max})$ can be used to find the optimal solution for the optimization problem (46).

C. Covert Rate Analysis

This section explores the impact of some critical parameters on the covert rate performance and corresponding performance optimization under the FD, HD, and general modes. Unless stated otherwise, the parameter values are provided in Table II.

We first explore the impact of the transmit power of DT P_t on covert rates under the three modes. Fig. 3 summarizes how covert rates vary with P_t for the setting of the transmit power of CE $P_c = \{1.0, 1.5\}$ W. It can be observed from Fig. 3 that as

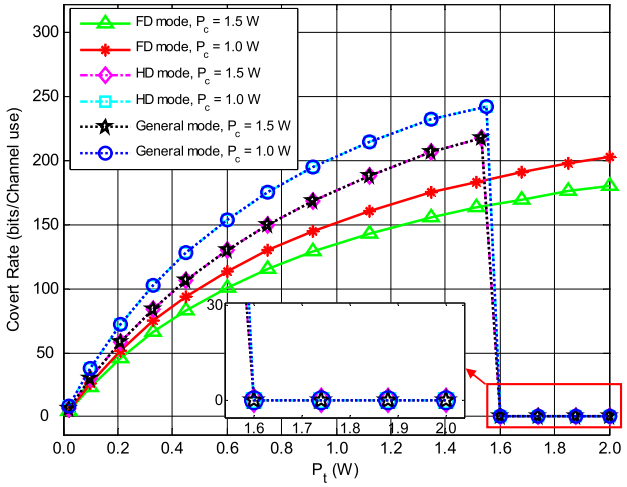

Fig. 3. Covert rates versus the transmit power of DT P_t under the FD, HD, and general modes.

P_t increases, the covert rate η_{FD} under the FD increases, while the covert rate η_{HD} under the HD mode first increases and then remains at zero. This is because the effect of increasing P_t is twofold. On the one hand, it can increase the covert rates under the two modes. On the other hand, it can also increase the probability that the warden WD detects the transmission of DT. When WD can detect its transmission, η_{HD} remains at zero. However, the receiver DR works in the FD mode, and thus, the interference emitted by DR can confuse the detection of WD, which leads to the increase of η_{FD} as P_t continues to increase. We know that the covert rate under the general mode corresponds to the maximum value of η_{FD} and η_{HD} as shown in Fig. 3. We further observe from Fig. 3 that for each fixed P_t, η_{HD} is higher than η_{FD} due to the self-interference under the FD mode. We can also observe from Fig. 3 that for each fixed P_t, the maximum covert rate with the setting of $P_c = 1.5$ W is smaller than that with the setting of $P_c = 1.0$ W for each mode. The reason behind this is that a large P_c can cause more interference to the DR, which leads to a small maximum covert rate.

We further investigate the impact of the covert requirement ε on covert rates under these three modes. We summarize in Fig. 4 how covert rates vary with ε for the setting of the transmit power of DT $P_t = \{1.0, 1.5\}$ W. We can see from Fig. 4 that as ε increases, η_{FD} increases, while η_{HD} first keeps at zero and then increases. The phenomenon can be explained as follows. We know that an increase of ε leads to the increases of η_{FD} and η_{HD}. However, as ε is relatively small, the covert constraint under the HD mode cannot be satisfied, and thus, η_{HD} is zero. As for the FD mode, the covert constraint is satisfied with the help of interference from DR. We can also see from Fig. 4 that the covert rate under the general mode is the maximum one of η_{FD} and η_{HD} for each fixed ε. We can also observe from Fig. 4 that for each ε, the maximum covert rate with the setting of $P_t = 1.5$ W is larger than that with the setting of $P_t = 1.0$ W for each mode. The reason behind this phenomenon is that a larger P_t results in a stronger received signal at the DR, which leads to the improvement of covet performance.

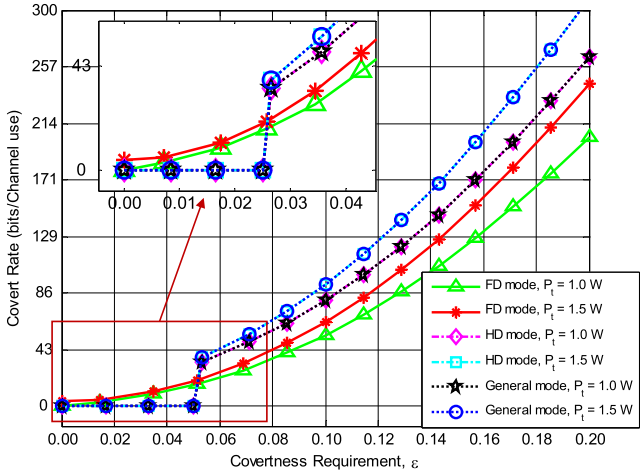

Fig. 4. Covert rates versus the covertness requirement ε under the FD, HD, and general modes.

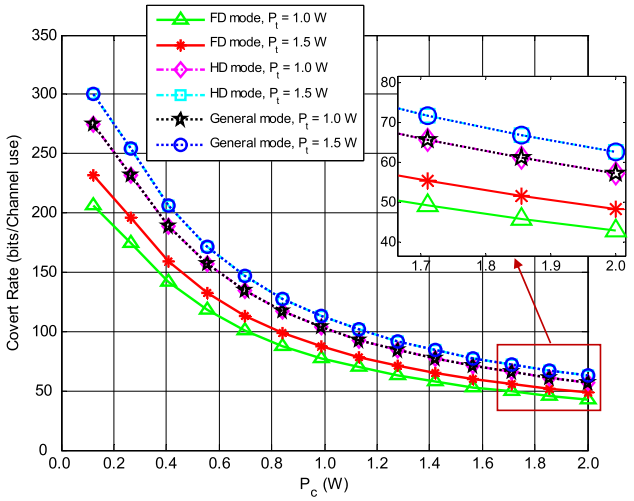

Fig. 5. Covert rates versus the transmit power of CE P_c under the FD, HD, and general modes.

We now explore the impact of the transmit power of CE P_c on covert rates for the setting of the transmit power of DT $P_t = \{1.0, 1.5\}$ W under these three modes, as shown in Fig. 5. It can be seen from Fig. 5 that the covert rates under these three modes decrease with the increase of P_c. This is because increasing P_c can increase the interference to the receiver DR, which leads to the decrease of the covert rates under these three modes. It can also seen from Fig. 5 that for each fixed P_c, the maximum covert rate with the setting of $P_t = 1.5$ W is larger than that with the setting of $P_t = 1.0$ W for each mode. The reason is the same as that in Fig. 4.

Finally, we examine the impact of the transmit maximum power of DR $P_{\max}$ on the covert rates under these three modes. Fig. 6 illustrates how the covert rates vary with $P_{\max}$ for the setting of the transmit power of DT $P_t = \{1.0, 1.5\}$ W. One observation from Fig. 6 indicates that as $P_{\max}$ increases, η_{FD} first remains at zero, then achieves a maximum value and finally decreases. Meanwhile, η_{HD} always remains at zero. This is due to the following reason. When $P_{\max}$ is relatively small, the covert constraints under the FD and HD modes

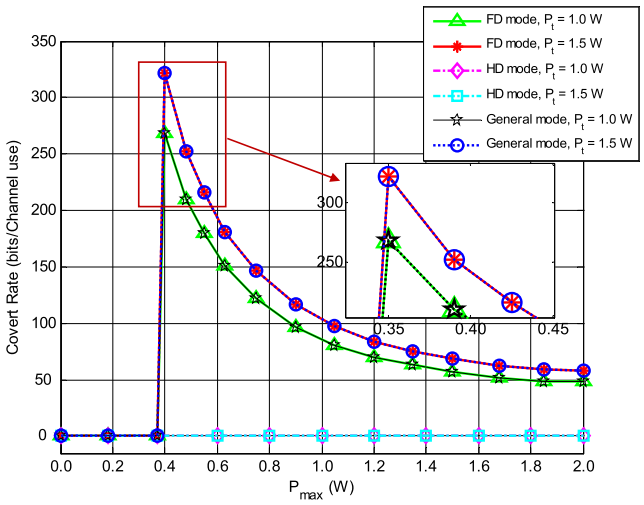

Fig. 6. Covert rates versus the transmit power of DR $P_{\max}$ under the FD, HD, and general modes.

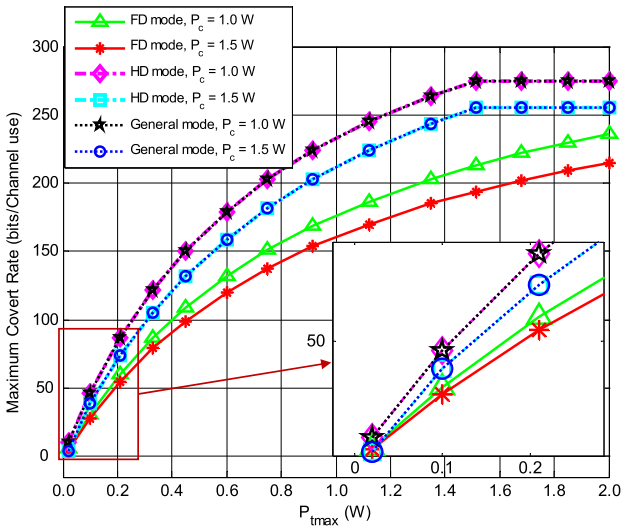

Fig. 7. Maximum covert rates versus the maximum transmit power of DT $P_{t\max}$ under the FD, HD, and general modes.

cannot be satisfied, and thus, both η_{FD} and η_{HD} remain at zero. When $P_{\max}$ increases up to a threshold, the covert constraint under the FD mode can be satisfied with the help of the artificial noise, which leads to a maximum covert rate. On the other hand, increasing $P_{\max}$ can also increase the self-interference at DR, which leads to the decrease of covert rate under the FD mode. Note that there is no effect of the artificial noise/self-interference under the HD mode, and thus, η_{HD} still remains at zero. It can also seen from Fig. 6 that for each fixed $P_{\max}$, the maximum covert rate with the setting of $P_t = 1.5$ W is larger than that with the setting of $P_t = 1.0$ W for each mode. The reason has been explained in Figs. 4 and 5.

D. Covert Rate Optimization

This section explores the impact of system parameters on the maximum covert rates under the FD, HD, and general modes.

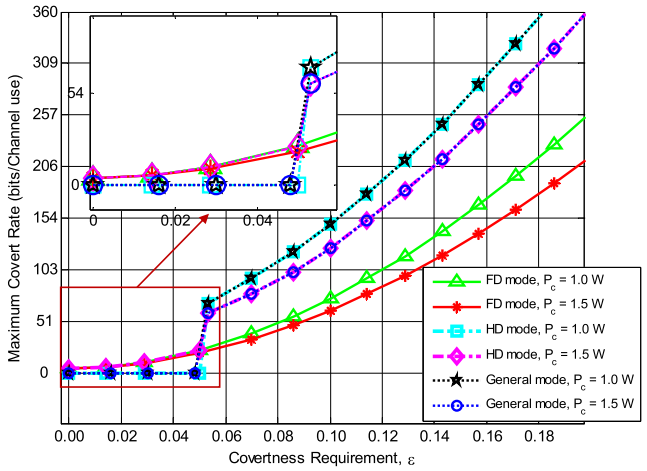

Fig. 8. Maximum covert rates versus the covertness requirement ε under the FD, HD, and general modes.

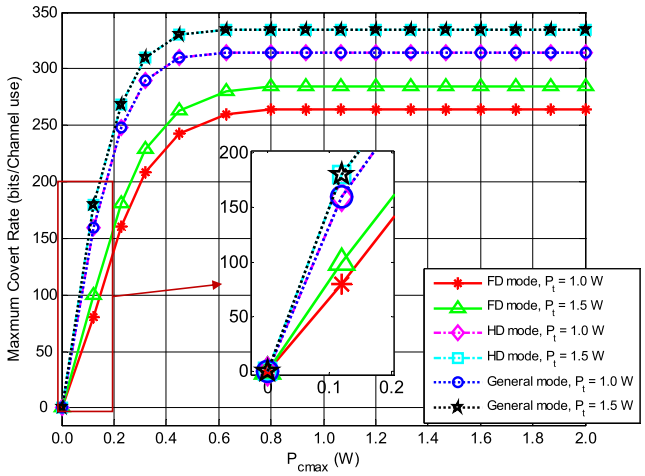

Fig. 9. Maximum covert rates versus the maximum transmit power of CE $P_{c\max}$ under the FD, HD, and general modes.

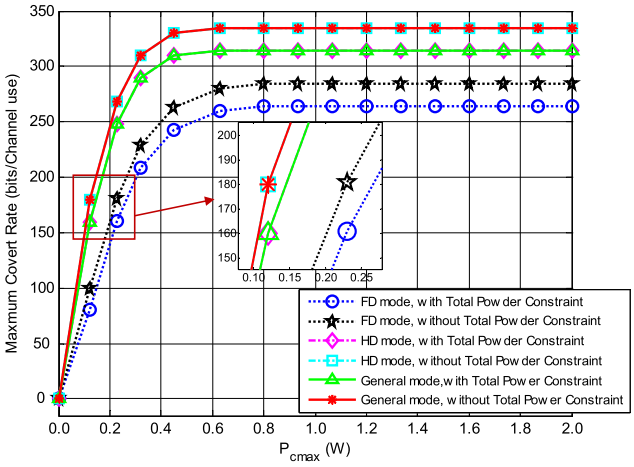

Fig. 10. Impact of $P_{\max}$ on maximum covert rate with/without the constraints of data rate and total power.

We summarize in Fig. 7 how the maximum covert rates vary with $P_{t\max}$ under these three modes with the setting of the transmit power of CE $P_c = \{1.0, 1.5\}$ W. We can see from Fig. 7 that for a given P_c, as $P_{t\max}$ increases, the maximum covert rates increase under the three modes, while as $P_{t\max}$ increases up to some threshold, the maximum covert rates under the HD and general modes keep unchanged. This is due to the following reason. As $P_{t\max}$ is relatively small, P_t has not reached the optimal value corresponding to the maximum value of the maximum covert rates. Thus, the maximum covert rates increase with the increase of $P_{t\max}$ under the three modes. As $P_{t\max}$ becomes larger, P_t reaches the optimal value and keeps unchanged under the HD and general modes, at which the maximum covert rates remain at the largest constant. However, due to the effect of self-interference under the FD mode, P_t has not reached the optimal value. Thus, the maximum covert rate under the FD mode increases with the increase of P_t. We can also observe from Fig. 7 that for each fixed $P_{t\max}$, the maximum covert rates with the setting of $P_c = 1.5$ W are smaller than these with the setting of $P_c = 1.0$ W under these three modes. This is due to the fact that a large P_c can cause more interference to the DR, which leads to small maximum covert rates under these three modes.

Fig. 8 illustrates how the maximum covert rates vary with the covertness requirement ε under these three modes with the setting of the transmit power of CE $P_c = \{1.0, 1.5\}$ W. It can be observed from Fig. 8 that as ε increases, the maximum covert rates under the FD and general modes increase, while the maximum covert rate under the HD mode first remains at zero and then increases. The reason behind this phenomenon is the same as that of Fig. 4. Similar to Fig. 7, we can see from Fig. 8 that for each fixed ε, the maximum covert rates with the setting of $P_c = 1.5$ W are smaller than these with the setting of $P_c = 1.0$ W under these three modes.

We proceed to explore the impact of $P_{c\max}$ on the maximum covert rates under these three modes with the setting of the transmit power of DT $P_t = \{1.0, 1.5\}$ W. It can be seen from Fig. 9 that as $P_{c\max}$ increases, the maximum covert rates under these three modes first increase, then achieve maximum values and keep unchanged. This can be explained as follows. According to the definition of covert rate, we know that the maximum covert rate under each mode is inversely proportional to the transmission outage probability of the cellular link from CE to BS. Increasing $P_{c\max}$ can reduce the transmission outage probability, which leads to the increase of the maximum covert rate under each mode. On the other hand, it can also incur more interference to the D2D link from DT to DR, which leads to the decrease of the maximum covert rate. As $P_{c\max}$ is relatively small, the former dominates the latter, and thus, the maximum covert rate under each mode increases with the increase of $P_{c\max}$. As $P_{c\max}$ further increases, the maximum covert rate achieves a maximum value and thus keeps unchanged under each mode. We can also observe from Fig. 9 that the maximum covert rates with the setting of $P_t = 1.5$ W are higher than these with the setting of $P_t = 1.0$ W under these three modes. This is because a large P_t leads to a high SINR at DR, which leads to a large maximum covert rate under each mode when the constraint of covert requirement can be satisfied.

To explore the tradeoff among the data rate, energy efficiency, and covert rate, we summarize in Fig. 10 how $P_{\max}$

affects the maximum covert rate with/without the constraints of data rate and total power for these three modes. We can see from Fig. 10 that as $P_{\max}$ increases, the maximum covert rates under all three modes without the constraint are always greater than that with the constraint. This is because the constraint of data rate and total power leads to the decrease of maximum covert rate, which achieves the tradeoff among the data rate, energy efficiency, and covert rate.

VII. Conclusion

In this article, we investigated the covert rate performance in an FD DCNT. We theoretically model the covert rate under the FD and HD modes, respectively. Then, we optimize the transmit powers of DT, DR, and CE for maximizing the corresponding covert rate. Specially, we designed a general mode to improve such performance. Remarkably, the extensive numerical simulations illustrate that our proposed general mode can achieve significant improvement in covert rate performance compared to pure HD mode or FD mode. An interesting future work is to explore the impact of node mobility on covert rate performance in DCNTs. Another promising work is to focus on the studies of covert rate performance in the multiuser scenario, where one D2D pair may be detected by more than one warden and one warden may be confused by more than one D2D receiver. Further, it is deserved to explore the covert communications of the complex multilevel structure with obstacles in our future study.

Appendix A
Proof of Theorem 1

Proof: Based on a step-by-step manner [49], we solve the optimization problem of (22). We first determine the monotonicity of η_{FD} with respect to P_t, and the monotonicity of $\mathcal{D}(P_0^{\mathrm{FD}}\|P_1^{\mathrm{FD}})$ with respect to P_t and P_c, respectively. Then, we derive the optimal transmit powers of DT and CE. Finally, we derive the optimal maximum transmit power of DR, i.e., $P_{\max}$.

A. Monotonicity of η_{FD}

To determine the nonotonicity of η_{FD} with respect to P_t, we first calculate the first derivative of γ_r^{FD} with respect to P_t in (16) as

$$\left(\gamma_r^{\mathrm{FD}}\right)'\big|_{P_t} = \frac{|h_{tr}|^2}{\phi|h_{rr}|^2P_r + |h_{cr}|^2P_c + \sigma_r^2} > 0. \tag{47}$$

Thus, γ_r^{FD} monotonically increases with P_t.

Then, we determine the monotonicity of δ_r^{FD} with respect to γ_r^{FD}.

According to [54], we know that

$$\delta_r^{\mathrm{FD}} \approx Q\left(f\left(\gamma_r^{\mathrm{FD}}, n, \zeta_{tr}\right)\right) \tag{48}$$

where

$$Q(x) = \int_x^{+\infty} \frac{1}{\sqrt{2\pi}} \exp\left(-\frac{t^2}{2}\right) dt \tag{49}$$

and

$$f\left(\gamma_r^{\mathrm{FD}}, n, \zeta_{tr}\right) = \ln 2 \sqrt{\frac{n}{1-\left(1+\gamma_r^{\mathrm{FD}}\right)^{-2}}}\left(\log_2\left(1+\gamma_r^{\mathrm{FD}}\right) - \zeta_{tr}\right). \tag{50}$$

We now derive the first derivative of δ_r^{FD} with respect to γ_r^{FD}, and then

$$\left(\delta_r^{\mathrm{FD}}\right)'\Big|_{\gamma_r^{\mathrm{FD}}} = -\frac{\exp\left[-\left(\frac{1}{2}f^2\left(\gamma_r^{\mathrm{FD}}, n, \zeta_{tr}\right)\right)\right]}{\sqrt{2\pi}} \times \sqrt{\frac{n}{\left(1+\gamma_r^{\mathrm{FD}}\right)^2-1}}\left[1 - \ln 2 \frac{\log_2\left(1+\gamma_r^{\mathrm{FD}}\right) - \zeta_{tr}}{\left(1+\gamma_r^{\mathrm{FD}}\right)^2-1}\right]. \tag{51}$$

To determine (51), let

$$h(x) = \frac{\log_2 x}{x^2-1} \tag{52}$$

where $x = 1+\gamma_r^{\mathrm{FD}} > 1$. We determine the first derivative of $h(x)$ as follows:

$$h'(x) = \frac{\frac{1}{\ln 2}\left(x - \frac{1}{x}\right) - 2x\log_2 x}{\left(x^2-1\right)^2}. \tag{53}$$

We can see that the sign of $h'(x)$ is the same as

$$v(x) = \frac{1}{\ln 2}\left(x - \frac{1}{x}\right) - 2x\log_2 x. \tag{54}$$

We further derive the first derivative of $v(x)$ with respect to x, and then

$$v'(x) = -\frac{1}{\ln 2}\left(1 - \frac{1}{x^2}\right) - 2\log_2 x < 0. \tag{55}$$

Thus, $v(x)$ decreases with x, where $x > 1$. Since $v(x) < v(1) = 0$, we have $h'(x) < 0$. Thus, $h(x)$ is a decreasing function of x. We use $h_{\max}(x)$ to denote the maximum value of $h(x)$. Then

$$h_{\max}(x) = \lim_{x\to 1} h(x) = \frac{1}{2\ln 2}. \tag{56}$$

Thus, regarding (51), we have

$$\ln 2 \frac{\log_2\left(1+\gamma_r^{\mathrm{FD}}\right) - \zeta_{tr}}{\left(1+\gamma_r^{\mathrm{FD}}\right)^2-1} \le \ln 2 \frac{\log_2\left(1+\gamma_r^{\mathrm{FD}}\right)}{\left(1+\gamma_r^{\mathrm{FD}}\right)^2-1} < \ln 2 \frac{1}{2\ln 2} = \frac{1}{2} \tag{57}$$

and then

$$1 - \ln 2 \frac{\log_2\left(1+\gamma_r^{\mathrm{FD}}\right) - \zeta_{tr}}{\left(1+\gamma_r^{\mathrm{FD}}\right)^2-1} > 1 - \frac{1}{2} > 0. \tag{58}$$

We obtain $(\delta_r^{\mathrm{FD}})'|_{\gamma_r^{\mathrm{FD}}} < 0$. Thus, δ_r^{FD} monotonically decreases with γ_r^{FD}. Similarly, δ_b^{FD} monotonically decreases with γ_b^{FD}.

We further calculate the first derivative of η_{FD} with respect to δ_r^{FD} as follows:

$$\left(\eta^{\mathrm{FD}}\right)'\Big|_{\delta_r^{\mathrm{FD}}} = -R_{\mathrm{FD}}\left(1-\delta_b^{\mathrm{FD}}\right) < 0. \tag{59}$$

Thus, η_{FD} deceases with δ_r^{FD}.

Finally, we obtain that η_{FD} monotonically increases with P_t.

B. Monotonicity of $\mathcal{D}(P_0^{FD}\|P_1^{FD})$

We calculate the first derivative of $\mathcal{D}(P_0^{\mathrm{FD}}\|P_1^{\mathrm{FD}})$ with respect to γ_w^{FD} as

$$D'\left(P_0^{\mathrm{FD}}\middle\|P_1^{\mathrm{FD}}\right)\Big|_{\gamma_w^{\mathrm{FD}}}=\frac{n\gamma_w^{\mathrm{FD}}}{\left(\gamma_w^{\mathrm{FD}}+1\right)^2}>0. \tag{60}$$

We continue to calculate the first derivative of γ_w^{FD} with respect to P_t, P_r, and P_c, respectively. Then, we have

$$\left(\gamma_w^{\mathrm{FD}}\right)'|_{P_t}=\frac{|h_{tw}|^2}{P_r|h_{rw}|^2+P_c|h_{cw}|^2+\sigma_w^2}>0 \tag{61}$$

$$\left(\gamma_w^{\mathrm{FD}}\right)'|_{P_r}=-\frac{P_t|h_{tw}|^2|h_{rw}|^2}{\left(P_r|h_{rw}|^2+P_c|h_{cw}|^2+\sigma_w^2\right)^2}<0 \tag{62}$$

and

$$\left(\gamma_w^{\mathrm{FD}}\right)'|_{P_c}=-\frac{P_t|h_{tw}|^2|h_{cw}|^2}{\left(P_r|h_{rw}|^2+P_c|h_{cw}|^2+\sigma_w^2\right)^2}<0. \tag{63}$$

Thus, $\mathcal{D}(P_0^{\mathrm{FD}}\|P_1^{\mathrm{FD}})$ monotonically increases with P_t, while monotonically decreases with P_r and P_c, respectively.

C. Optimal Transmit Power of DT

Since both the objective function η_{FD} and $\mathcal{D}(P_0^{\mathrm{FD}}\|P_1^{\mathrm{FD}})$ in the constraint of (22b) monotonically increase with P_t, we can determine the optimal value P_t^* of P_t for maximizing η_{FD} and ensuring $\mathcal{D}(P_0^{\mathrm{FD}}\|P_1^{\mathrm{FD}})=2\varepsilon^2$ with any given P_r an P_c.

Substituting (12) into $\mathcal{D}(P_0^{\mathrm{FD}}\|P_1^{\mathrm{FD}})=2\varepsilon^2$, we have

$$n\left[\ln\left(1+\gamma_w^{\mathrm{FD}}\right)-\frac{\gamma_w^{\mathrm{FD}}}{1+\gamma_w^{\mathrm{FD}}}\right]=2\varepsilon^2. \tag{64}$$

To guarantee a low detection probability at WD, γ_w^{FD} is normally very small. Thus, $\ln(1+x)\approx x$. Then, (64) can be rewritten as follows:

$$n\left(\gamma_w^{\mathrm{FD}}-\frac{\gamma_w^{\mathrm{FD}}}{1+\gamma_w^{\mathrm{FD}}}\right)=2\varepsilon^2. \tag{65}$$

By solving (65), we have

$$\gamma_w^{\mathrm{FD}}=\frac{\varepsilon^2+\sqrt{\varepsilon^4+2\varepsilon^2 n}}{n}. \tag{66}$$

Substituting (24) into (66), we have

$$\frac{|h_{tw}|^2P_t}{|h_{cw}|^2P_c+|h_{rw}|^2P_r+\sigma_w^2}=\frac{\varepsilon^2+\sqrt{\varepsilon^4+2\varepsilon^2 n}}{n} \tag{67}$$

and thus, we obtain the optimal P_t^* given in (25).

D. Optimal Transmit Powers of CE

We know that δ_r^{FD} and δ_b^{FD} monotonically decreases with γ_r^{FD} and γ_b^{FD}, respectively. We can also determine the first derivative of η_{FD} with respect to δ_b^{FD} as

$$\left(\eta^{\mathrm{FD}}\right)'\Big|_{\delta_b^{\mathrm{FD}}}=-R_{\mathrm{FD}}\left(1-\delta_r^{\mathrm{FD}}\right)<0. \tag{68}$$

Thus, based on (59), we obtain that η^{FD} decreases with δ_r^{FD} and δ_b^{FD}, respectively. Then, η^{FD} monotonically increases with γ_r^{FD} and γ_b^{FD}, respectively.

Based on (67), we have

$$P_t=\frac{\varepsilon^2+\sqrt{\varepsilon^4+2\varepsilon^2 n}}{n}\cdot\frac{|h_{cw}|^2P_c+|h_{rw}|^2P_r+\sigma_w^2}{|h_{tw}|^2} \tag{69}$$

and

By substituting (69) into (16), we have

$$\gamma_r^{\mathrm{FD}}=\frac{\varepsilon^2+\sqrt{\varepsilon^4+2\varepsilon^2 n}}{n}\times\frac{|h_{tr}|^2\left(|h_{cw}|^2P_c+|h_{rw}|^2P_r+\sigma_w^2\right)}{|h_{tw}|^2\left(|h_{rr}|^2\phi P_r+|h_{cr}|^2P_c+\sigma_r^2\right)}. \tag{70}$$

We now calculate the first derivative of γ_r^{FD} with respect to P_c as follows:

$$\left(\gamma_r^{\mathrm{FD}}\right)'|_{P_c}=\frac{\varepsilon^2+\sqrt{\varepsilon^4+2\varepsilon^2 n}}{n}\cdot\frac{|h_{tr}|^2}{|h_{tw}|^2}\times\frac{\left(|h_{rr}|^2|h_{cw}|^2\phi P_r+\sigma_r^2|h_{cw}|^2-|h_{rw}|^2|h_{cr}|^2P_r-|h_{cr}|^2\sigma_w^2\right)}{\left(|h_{cr}|^2P_c+|h_{rr}|^2\phi P_r+\sigma_r^2\right)^2}. \tag{71}$$

Note that the sign of γ_r^{FD} is solely determined by the term of $|h_{rr}|^2|h_{cw}|^2\phi P_r+\sigma_r^2|h_{cw}|^2-|h_{rw}|^2|h_{cr}|^2P_r-|h_{cr}|^2\sigma_w^2$. Meanwhile, we can see from (15) that γ_b^{FD} monotonically increases with P_c. We need to discuss the following two cases.

Case 1: When $|h_{rr}|^2|h_{cw}|^2\phi P_r+\sigma_r^2|h_{cw}|^2\geq|h_{rw}|^2|h_{cr}|^2P_r+|h_{cr}|^2\sigma_w^2$, we have $(\gamma_r^{\mathrm{FD}})'|_{P_c}.\geq 0$, which means that γ_r^{FD} monotonically increases with P_c. Thus, we obtain $P_c^*=P_{c\max}$.

Case 2: When $|h_{rr}|^2|h_{cw}|^2\phi P_r+\sigma_r^2|h_{cw}|^2<|h_{rw}|^2|h_{cr}|^2P_r+|h_{cr}|^2\sigma_w^2$, we have $(\gamma_r^{\mathrm{FD}})'|_{P_c}.<0$, which means that γ_r^{FD} monotonically decreases with P_c. Thus, we obtain $P_c^*=0$.

E. Optimal the Maximum Transmit Power of DR

Substituting (15) and (16) into (14) we have

$$\eta_{\mathrm{FD}}=R_{\mathrm{FD}}\frac{\lambda_{tb}\lambda_{rb}\lambda_{rr}\lambda_{cr}\exp\left[-\left(\alpha\sigma_b^2+\beta\sigma_r^2\right)\right]}{\alpha\beta^2\phi(P_t+\lambda_{tb})(P_c+\lambda_{cr})}\cdot\nu(P_{\max}) \tag{72}$$

where

$$\nu(P_{\max})=\frac{1}{P_{\max}^2}\ln\left(1+\frac{\alpha P_{\max}}{\lambda_{tb}}\right)\ln\left(1+\frac{\beta\phi P_{\max}}{\lambda_{rr}}\right). \tag{73}$$

Then, we need to find an optimal $P_{\max}$ to maximize the covert rate η_{FD}, This corresponds to the case that determining an optimal $P_{\max}$ maximizes $\nu(P_{\max})$, which can be easily solved by a 1-D search method. We complete the proof of Theorem 1. ■

Appendix B
Proof of Theorem 2

Proof: Using the step-by-step manner, we solve this optimization problem. We first determine the monotonicity of $\mathcal{D}(P_0^{\mathrm{HD}}\|P_1^{\mathrm{HD}})$ with respect to P_t and P_c. To this end, we calculate the first derivative of $\mathcal{D}(P_0^{\mathrm{HD}}\|P_1^{\mathrm{HD}})$ with respect to γ_w^{HD} as follows:

$$D'\left(P_0^{\mathrm{HD}}\middle\|P_1^{\mathrm{HD}}\right)\Big|_{\gamma_w^{\mathrm{HD}}}=\frac{n\gamma_w^{\mathrm{HD}}}{\left(\gamma_w^{\mathrm{HD}}+1\right)^2}>0. \tag{74}$$

Thus, $\mathcal{D}(P_0^{\mathrm{HD}}\|P_1^{\mathrm{HD}})$ monotonically increases with γ_w^{HD}.

We now continue to calculate the monotonicity of γ_w^{HD} with respect to P_t and P_c by solving its first derivative. Then, we have

$$\left(\gamma_w^{\mathrm{HD}}\right)'|_{P_t} = \frac{|h_{tw}|^2}{P_c|h_{cw}|^2 + \sigma_w^2} > 0 \tag{75}$$

and

$$\left(\gamma_w^{\mathrm{HD}}\right)'|_{P_c} = -\frac{P_t|h_{tw}|^2|h_{cw}|^2}{\left(P_c|h_{cw}|^2 + \sigma_w^2\right)^2} < 0. \tag{76}$$

Thus, we obtain that γ_w^{HD} monotonically increases with P_t, while decreases with P_c. Accordingly, $\mathcal{D}(P_0^{\mathrm{HD}}\|P_1^{\mathrm{HD}})$ monotonically increases with P_t and decreases with P_c.

Based on the fact that both $\mathcal{D}(P_0^{\mathrm{HD}}\|P_1^{\mathrm{HD}})$ and η_{HD} are increasing functions of P_t, we know that regarding an optimal value P_t^* of P_t, the constraint $\mathcal{D}(P_0^{\mathrm{HD}}\|P_1^{\mathrm{HD}}) \le 2\varepsilon^2$ is always guaranteed for any fixed P_c and P_r. We now determine the optimal P_t^*.

Substituting (36) into $\mathcal{D}(P_0^{\mathrm{HD}}\|P_1^{\mathrm{HD}}) = 2\varepsilon^2$, we have

$$n\left[\ln\left(1+\gamma_w^{\mathrm{HD}}\right) - \frac{\gamma_w^{\mathrm{HD}}}{1+\gamma_w^{\mathrm{HD}}}\right] = 2\varepsilon^2. \tag{77}$$

Using x to approximate $\ln(1+x)$, (77) can rewritten as follows:

$$n\left(\gamma_w^{\mathrm{HD}} - \frac{\gamma_w^{\mathrm{HD}}}{1+\gamma_w^{\mathrm{HD}}}\right) = 2\varepsilon^2. \tag{78}$$

By solving (78), we have

$$\gamma_w^{\mathrm{HD}} = \frac{\varepsilon^2 + \sqrt{\varepsilon^4 + 2\varepsilon^2 n}}{n}. \tag{79}$$

By substituting (37) into (79), we obtain

$$\frac{|h_{tw}|^2 P_t}{|h_{cw}|^2 P_c + \sigma_w^2} = \frac{\varepsilon^2 + \sqrt{\varepsilon^4 + 2\varepsilon^2 n}}{n}. \tag{80}$$

Thus, the optimal P_t^* can be obtained in (38).

We proceed to derive the optimal P_c^*. Since δ_r^{HD} monotonically decreases with γ_r^{HD}, the objective function η^{HD} monotonically increases with γ_r^{HD}. We only need to determine the monotonicity of γ_r^{HD} with respect to P_c.

Based on (30) and (80), γ_r^{HD} can be expressed as follows:

$$\gamma_r^{\mathrm{HD}} = \frac{\varepsilon^2 + \sqrt{\varepsilon^4 + 2\varepsilon^2 n}}{n} \cdot \frac{|h_{tr}|^2\left(|h_{cw}|^2 P_c + \sigma_w^2\right)}{|h_{tw}|^2\left(|h_{cr}|^2 P_c + \sigma_r^2\right)}. \tag{81}$$

We calculate the first derivative of γ_r^{HD} with respect to P_c as follows:

$$\left(\gamma_r^{\mathrm{HD}}\right)'|_{P_c} = \frac{\varepsilon^2 + \sqrt{\varepsilon^4 + 2\varepsilon^2 n}}{n} \cdot \frac{|h_{tr}|^2}{|h_{tw}|^2} \times \frac{\left(|h_{cw}|^2\sigma_r^2 - |h_{cr}|^2\sigma_w^2\right)}{\left(|h_{cr}|^2 P_c + \sigma_r^2\right)^2}. \tag{82}$$

Note that the sign of γ_r^{HD} is solely determined by the term of $(|h_{cw}|^2\sigma_r^2 - |h_{cr}|^2\sigma_w^2)$. Thus, we consider the following two cases.

Case 1: When $|h_{cw}|^2\sigma_r^2 \ge |h_{cr}|^2\sigma_w^2$, we have $(\gamma_r^{\mathrm{HD}})'|_{P_c} \ge 0$. Thus, γ_r^{HD} monotonically increases with P_c. Since the first derivative of γ_b^{HD} in (29) is determined as follows:

$$\left(\gamma_b^{\mathrm{HD}}\right)'|_{P_c} = \frac{|h_{cb}|^2}{|h_{tb}|^2 P_t + \sigma_b^2} > 0 \tag{83}$$

γ_b^{HD} monotonically increases with P_c. Finally, we obtain $P_c^* = P_{c\max}$.

Case 2: When $|h_{cw}|^2\sigma_r^2 < |h_{cr}|^2\sigma_w^2$, we have $(\gamma_r^{\mathrm{HD}})'|_{P_c} < 0$. Thus, γ_r^{HD} monotonically decreases with P_c. To achieve the maximization of η_{HD}, P_c needs to set as small as possible. So, we have $P_c^* = 0$. Then, (38) and (39) follow. We complete the proof of Theorem 2. ■

REFERENCES

[1] B. Yang, T. Taleb, Y. Shen, X. Jiang, and W. Yang, "Performance, fairness, and tradeoff in UAV swarm underlaid mmWave cellular networks with directional antennas," *IEEE Trans. Wireless Commun.*, vol. 20, no. 4, pp. 2383–2397, Apr. 2021.

[2] M. Haus, M. Waqas, A. Y. Ding, Y. Li, S. Tarkoma, and J. Ott, "Security and privacy in device-to-device (D2D) communication: A review," *IEEE Commun. Surveys Tuts.*, vol. 19, no. 2, pp. 1054–1079, 2nd Quart., 2017.

[3] P. Khuntia and R. Hazra, "An efficient channel and power allocation scheme for D2D enabled cellular communication system: An IoT application," *IEEE Sensors J.*, vol. 21, no. 22, pp. 25340–25351, Nov. 2021.

[4] S. W. H. Shah, M. M. U. Rahman, A. N. Mian, O. A. Dobre, and J. Crowcroft, "Effective capacity analysis of HARQ-enabled D2D communication in multi-tier cellular networks," *IEEE Trans. Veh. Technol.*, vol. 70, no. 9, pp. 9144–9159, Sep. 2021.

[5] B. Yang, T. Taleb, Z. Wu, and L. Ma, "Spectrum sharing for secrecy performance enhancement in D2D-enabled UAV networks," *IEEE Netw.*, vol. 34, no. 6, pp. 156–163, Nov./Dec. 2020.

[6] R. Sun, B. Yang, S. Ma, Y. Shen, and X. Jiang, "Covert rate maximization in wireless full-duplex relaying systems with power control," *IEEE Trans. Commun.*, vol. 69, no. 9, pp. 6198–6212, Sep. 2021.

[7] S. Yan, X. Zhou, J. Hu, and S. V. Hanly, "Low probability of detection communication: Opportunities and challenges," *IEEE Wireless Commun.*, vol. 26, no. 5, pp. 19–25, Oct. 2019.

[8] Y. Jiang, L. Wang, H. Zhao, and H.-H. Chen, "Covert communications in D2D underlaying cellular networks with power domain NOMA," *IEEE Syst. J.*, vol. 14, no. 3, pp. 3717–3728, Sep. 2020.

[9] H. Rao, M. Wu, J. Wang, W. Tang, S. Xiao, and S. Li, "D2D covert communications with safety area," *IEEE Syst. J.*, vol. 15, no. 2, pp. 2331–2341, Jun. 2021.

[10] Y. Jiang, L. Wang, and H.-H. Chen, "Covert communications in D2D underlaying cellular networks with antenna array assisted artificial noise transmission," *IEEE Trans. Veh. Technol.*, vol. 69, no. 3, pp. 2980–2992, Mar. 2020.

[11] J. Li, D. Wu, C. Yue, Y. Yang, M. Wang, and F. Yuan, "Energy-efficient transmit probability-power control for covert D2D communications with age of information constraints," *IEEE Trans. Veh. Technol.*, vol. 71, no. 9, pp. 9690–9704, Sep. 2022.

[12] J. Li, M. Wang, Y. Wang, X. Shi, and W. Cheng, "Covert communications in D2D underlaying cellular networks with multiple wardens," in *Proc. Int. Conf. Wireless Commun. Signal Process. (WCSP)*, 2020, pp. 847–852.

[13] X. Shi, D. Wu, C. Yue, C. Wan, and X. Guan, "Resource allocation for covert communication in D2D content sharing: A matching game approach," *IEEE Access*, vol. 7, pp. 72835–72849, 2019.

[14] X. Shi, D. Wu, C. Wan, M. Wang, and Y. Zhang, "Trust evaluation and covert communication-based secure content delivery for D2D networks: A hierarchical matching approach," *IEEE Access*, vol. 7, pp. 134838–134853, 2019.

[15] S. Lee, R. J. Baxley, M. A. Weitnauer, and B. Walkenhorst, "Achieving undetectable communication," *IEEE J. Sel. Topics Signal Process.*, vol. 9, no. 7, pp. 1195–1205, Oct. 2015.

[16] B. He, S. Yan, X. Zhou, and V. K. N. Lau, "On covert communication with noise uncertainty," *IEEE Commun. Lett.*, vol. 21, no. 4, pp. 941–944, Apr. 2017.

[17] D. Wang, P. Qi, Y. Zhao, C. Li, W. Wu, and Z. Li, "Covert wireless communication with noise uncertainty in space-air-ground integrated vehicular networks," *IEEE Trans. Intell. Transp. Syst.*, vol. 23, no. 3, pp. 2784–2797, Mar. 2022.

[18] K. Shahzad and X. Zhou, "Covert wireless communications under quasi-static fading with channel uncertainty," *IEEE Trans. Inf. Forensics Security*, vol. 16, pp. 1104–1116, 2021.

[19] Z. Cheng et al., "Covert surveillance via proactive eavesdropping under channel uncertainty," *IEEE Trans. Commun.*, vol. 69, no. 6, pp. 4024–4037, Jun. 2021.

[20] B. He, S. Yan, X. Zhou, and H. Jafarkhani, "Covert wireless communication with a poisson field of interferers," *IEEE Trans. Wireless Commun.*, vol. 17, no. 9, pp. 6005–6017, Sep. 2018.

[21] T. V. Sobers, B. A. Bash, S. Guha, D. Towsley, and D. Goeckel, "Covert communication in the presence of an uninformed jammer," *IEEE Trans. Wireless Commun.*, vol. 16, no. 9, pp. 6193–6206, Sep. 2017.

[22] W. Liang, J. Shi, Z. Tie, and F. Yang, "Performance analysis for UAV-jammer aided covert communication," *IEEE Access*, vol. 8, pp. 111394–111400, 2020.

[23] C. Wang, Z. Li, and D. W. K. Ng, "Covert rate optimization of millimeter wave full-duplex communications," *IEEE Trans. Wireless Commun.*, vol. 21, no. 5, pp. 2844–2861, May 2022.

[24] W. Xiang, J. Wang, S. Xiao, and W. Tang, "Achieving constant rate covert communication via multiple antennas," in *Proc. IEEE 95th Veh. Technol. Conf. (VTC2022-Spring)*, 2022, pp. 1–6.

[25] J. Zhang et al., "Joint beam training and data transmission design for covert millimeter-wave communication," *IEEE Trans. Inf. Forensics Security*, vol. 16, pp. 2232–2245, 2021.

[26] J. Zhang, M. Li, M.-J. Zhao, X. Ji, and W. Xu, "Multi-user beam training and transmission design for covert millimeter-wave communication," *IEEE Trans. Inf. Forensics Security*, vol. 17, pp. 1528–1543, 2022.

[27] R. Ma, W. Yang, J. Hu, and X. Lu, "Covert mmWave communication when the warden locates in the beam direction," *IEEE Wireless Commun. Lett.*, vol. 11, no. 12, pp. 2595–2599, Dec. 2022.

[28] W. Gao, Y. Chen, C. Han, and Z. Chen, "Distance-adaptive absorption peak modulation (DA-APM) for Terahertz covert communications," *IEEE Trans. Wireless Commun.*, vol. 20, no. 3, pp. 2064–2077, Mar. 2021.

[29] S. Yan, Y. Cong, S. V. Hanly, and X. Zhou, "Gaussian signalling for covert communications," *IEEE Trans. Wireless Commun.*, vol. 18, no. 7, pp. 3542–3553, Jul. 2019.

[30] S. Yan, B. He, X. Zhou, Y. Cong, and A. L. Swindlehurst, "Delay-intolerant covert communications with either fixed or random transmit power," *IEEE Trans. Inf. Forensics Security*, vol. 14, no. 1, pp. 129–140, Jan. 2019.

[31] S. Yan, S. V. Hanly, and I. B. Collings, "Optimal transmit power and flying location for UAV covert wireless communications," *IEEE J. Sel. Areas Commun.*, vol. 39, no. 11, pp. 3321–3333, Nov. 2021.

[32] C. Huang, H. Huang, and A. V. Savkin, *Autonomous UAV Navigation for Covert Video Surveillance*. Hoboken, NJ, USA: Wiley, 2023, pp. 159–193.

[33] H. Huang, A. V. Savkin, and W. Ni, "Decentralized navigation of a UAV team for collaborative covert eavesdropping on a group of mobile ground nodes," *IEEE Trans. Autom. Sci. Eng.*, vol. 19, no. 4, pp. 3932–3941, Oct. 2022.

[34] X. Li, H. Huang, and A. V. Savkin, "Use of a UAV base station for searching and bio-inspired covert video surveillance of tagged wild animals," in *Proc. Aust. New Zealand Control Conf. (ANZCC)*, 2020, pp. 87–90.

[35] Y. Lin, L. Jin, K. Huang, Z. Zhong, and Q. Han, "Covert threat region analysis of 3-D location-based Beamforming in Rician channel," *IEEE Wireless Commun. Lett.*, vol. 11, no. 6, pp. 1253–1257, Jun. 2022.

[36] R. Xu, B. Zhang, D. Guo, H. Wang, and G. Ding, "Finite Blocklength covert communications: When the warden wants to detect the communications quickly," *IEEE Trans. Veh. Technol.*, vol. 71, no. 10, pp. 11278–11283, Oct. 2022.

[37] H. Q. Ta, K. Ho-Van, D. B. Da Costa, S. W. Kim, and H. Oh, "Covert communications over non-orthogonal multiple overt channels," *IEEE Access*, vol. 10, pp. 122361–122375, 2022.

[38] J. Hu, S. Yan, X. Zhou, F. Shu, and J. Wang, "Covert communication in wireless relay networks," in *Proc. IEEE Global Commun. Conf. (GLOBECOM)*, 2017, pp. 1–6.

[39] Y. Su, H. Sun, Z. Zhang, Z. Lian, Z. Xie, and Y. Wang, "Covert communication with relay selection," *IEEE Wireless Commun. Lett.*, vol. 10, no. 2, pp. 421–425, Feb. 2021.

[40] J. Wang, W. Tang, Q. Zhu, X. Li, H. Rao, and S. Li, "Covert communication with the help of relay and channel uncertainty," *IEEE Wireless Commun. Lett.*, vol. 8, no. 1, pp. 317–320, Feb. 2019.

[41] J. Hu, S. Yan, F. Shu, and J. Wang, "Covert transmission with a self-sustained relay," *IEEE Trans. Wireless Commun.*, vol. 18, no. 8, pp. 4089–4102, Aug. 2019.

[42] D. Deng, X. Li, S. Dang, M. C. Gursoy, and A. Nallanathan, "Covert communications in intelligent reflecting surface-assisted two-way relaying networks," *IEEE Trans. Veh. Technol.*, vol. 71, no. 11, pp. 12380–12385, Nov. 2022.

[43] M. T. Mamaghani and Y. Hong, "Aerial intelligent reflecting surface-enabled Terahertz covert communications in beyond-5G Internet of Things," *IEEE Internet Things J.*, vol. 9, no. 19, pp. 19012–19033, Oct. 2022.

[44] X. Chen, T.-X. Zheng, L. Dong, M. Lin, and J. Yuan, "Enhancing MIMO covert communications via intelligent reflecting surface," *IEEE Wireless Commun. Lett.*, vol. 11, no. 1, pp. 33–37, Jan. 2022.

[45] C. Wang, Z. Li, J. Shi, and D. W. K. Ng, "Intelligent reflecting surface-assisted multi-antenna covert communications: Joint active and passive Beamforming optimization," *IEEE Trans. Commun.*, vol. 69, no. 6, pp. 3984–4000, Jun. 2021.

[46] J. Jiang, J. Jing, R. Ma, B. Che, and W. Yang, "Covert relay communications with finite block-length against combining detection," *IEEE Wireless Commun. Lett.*, vol. 11, no. 11, pp. 2450–2454, Nov. 2022.

[47] A. Sheikholeslami, M. Ghaderi, D. Towsley, B. A. Bash, S. Guha, and D. Goeckel, "Multi-hop routing in covert wireless networks," *IEEE Trans. Wireless Commun.*, vol. 17, no. 6, pp. 3656–3669, Jun. 2018.

[48] H.-M. Wang, Y. Zhang, X. Zhang, and Z. Li, "Secrecy and covert communications against UAV surveillance via multi-hop networks," *IEEE Trans. Commun.*, vol. 68, no. 1, pp. 389–401, Jan. 2020.

[49] K. Shahzad, X. Zhou, S. Yan, J. Hu, F. Shu, and J. Li, "Achieving covert wireless communications using a full-duplex receiver," *IEEE Trans. Wireless Commun.*, vol. 17, no. 12, pp. 8517–8530, Dec. 2018.

[50] T.-X. Zheng, Z. Yang, C. Wang, Z. Li, J. Yuan, and X. Guan, "Wireless covert communications aided by distributed cooperative jamming over slow fading channels," *IEEE Trans. Wireless Commun.*, vol. 20, no. 11, pp. 7026–7039, Nov. 2021.

[51] J. Hu, K. Shahzad, S. Yan, X. Zhou, F. Shu, and J. Li, "Covert communications with a full-duplex receiver over wireless fading channels," in *Proc. IEEE Int. Conf. Commun. (ICC)*, 2018, pp. 1–6.

[52] L. Yang, W. Yang, S. Xu, L. Tang, and Z. He, "Achieving covert wireless communications using a full-duplex multi-antenna receiver," in *Proc. IEEE 5th Int. Conf. Comput. Commun. (ICCC)*, 2019, pp. 912–916.

[53] B. A. Bash, D. Goeckel, and D. Towsley, "Limits of reliable communication with low probability of detection on AWGN channels," *IEEE J. Sel. Areas Commun.*, vol. 31, no. 9, pp. 1921–1930, Sep. 2013.

[54] X. Sun, S. Yan, N. Yang, Z. Ding, C. Shen, and Z. Zhong, "Short-packet downlink transmission with non-orthogonal multiple access," *IEEE Trans. Wireless Commun.*, vol. 17, no. 7, pp. 4550–4564, Jul. 2018.

Yihuai Yang received the B.E. degree in communication engineering from Kunming University of Science and Technology, Kunming, China, in 2001, and the M.S. degree in communication and information system from Yunnan University, Kunming, in 2006.

She is an Associate Professor with the School of Information Engineering, Kunming University, Kunming. Her research interests include wireless channel characteristics, wireless body networks, and Internet of Things.

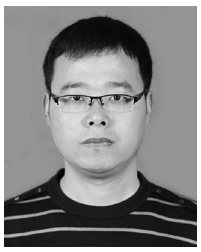

Bin Yang received the Ph.D. degree in systems information science from Future University Hakodate, Hakodate, Japan, in 2015.

He was a Research Fellow with the School of Electrical Engineering, Aalto University, Espoo, Finland, from July 2019 to November 2021. He is currently a Professor with the School of Computer and Information Engineering, Chuzhou University, Chuzhou, China, and also with the School of Information Engineering, Kunming University, Kunming, China. His research interests include unmanned aerial vehicle networks, cyber security, and Internet of Things.

Shikai Shen was born in 1964. He received the B.S. degree from Yunnan Normal University, Kunming, China, in 1984, and the M.S. degree from Yunnan University, Kunming, in 2003.

He is currently a Professor with Kunming University, Kunming. His research interests include wireless sensor networks, network coding, and Internet of Things.

Prof. Shen is a Senior Member of China Computer Federation.

Yumei She was born in 1965. She received the B.S. degree from Minzu University of China, Beijing, China, in 1985.

She is currently a Professor with Yunnan Minzu University, Kunming, Yunnan, China. Her research interests include natural language processing and wireless sensor networks.

Prof. She is a member of China Computer Federation.

Tarik Taleb (Senior Member, IEEE) received the B.E. degree (Distinction) in information engineering and the M.Sc. and Ph.D. degrees in information sciences from Tohoku University, Sendai, Japan, in 2001, 2003, and 2005, respectively.

He is currently a Professor with the Centre for Wireless Communications Networks and Systems Unit, Faculty of Information Technology and Electrical Engineering, The University of Oulu, Oulu, Finland. He is the Founder and the Director of the MOSA!C Lab, Oulu. From October 2014 and December 2021, he was a Professor with the School of Electrical Engineering, Aalto University, Espoo, Finland. Prior to that, he was working as a Senior Researcher and the 3GPP Standards Expert with NEC Europe Ltd., Heidelberg, Germany. Before joining NEC and till March 2009, he worked as an Assistant Professor with the Graduate School of Information Sciences, Tohoku University, in a lab fully funded by KDDI, the second largest mobile operator in Japan. From October 2005 to March 2006, he worked as a Research Fellow with the Intelligent Cosmos Research Institute, Sendai. His research interests lie in the field of telco cloud, network softwarization and network slicing, AI-based software-defined security, immersive communications, mobile multimedia streaming, and next-generation mobile networking.

Dr. Taleb served as the General Chair of the 2019 edition of the IEEE Wireless Communications and Networking Conference held in Marrakech, Morocco. He was the Guest Editor-in-Chief of the IEEE JOURNAL ON SELECTED AREAS IN COMMUNICATIONS Series on Network Softwarization and Enablers. He was on the editorial board of the IEEE TRANSACTIONS ON WIRELESS COMMUNICATIONS, *IEEE Wireless Communications Magazine*, IEEE INTERNET OF THINGS JOURNAL, IEEE TRANSACTIONS ON VEHICULAR TECHNOLOGY, IEEE COMMUNICATIONS SURVEYS AND TUTORIALS, and a number of Wiley journals. Till December 2016, he served as the Chair of the Wireless Communications Technical Committee. He has been also directly engaged in the development and standardization of the Evolved Packet System as a member of 3GPP's System Architecture working group 2.